FABRICATION AND CHARACTERISATION OF DYE SENSITISED SOLAR CELL

OON YEN HAN

A project report submitted in partial fulfilment of the requirements for the award of the degree of Bachelor (Hons.) of Materials and Manufacturing Engineering

Faculty of Engineering and Science
Universiti Tunku Abdul Rahman

April 2011

FDECLARATION

I hereby declare that this project report is based on my original work except for citations and quotations which have been duly acknowledged. I also declare that it has not been previously and concurrently submitted for any other degree or award at UTAR or other institutions.

Signature : _____

Name : Oon Yen Han

ID No. : 07 UEB 06019

Date : 16th May 2011

APPROVAL FOR SUBMISSION

I certify that this project report entitled **"FABRICATION AND CHARACTERISATION OF DYE SENSITISED SOLAR CELL"** was prepared by **OON YEN HAN** has met the required standard for submission in partial fulfilment of the requirements for the award of Bachelor (Hons.) of Materials and Manufacturing Engineering at Universiti Tunku Abdul Rahman.

Approved by,

Signature : _____

Supervisor : Assistant Professor Dr. Khaw Chwin Chieh

Date : _____

Specially dedicated to
my beloved mother and father

ACKNOWLEDGEMENTS

I would like to thank everyone who had contributed to the successful completion of this project. I would like to express my gratitude to my research supervisor, Assistant Professor Dr. Khaw Chwin Chieh and examiner Associate Professor Dr. Liang Meng Suan for their invaluable advice, guidance and their enormous patience throughout the development of the research.

In addition, I would also like to express my grateful appreciation to my loving parents who had helped and given me encouragement when I faced problems and bottlenecks. Additionally, I specially thank Ms. Shirley Law Sing Ling, Ms Li Hui and Ms. Joey, whose invaluable help has made this project success.

FABRICATION AND CHARACTERISATION OF DYE SENSITISED SOLAR CELL

ABSTRACT

With the high energy consumption nowadays, the amount of fossil fuel is depleted significantly. Scientists predicted that, with current consumption rate, reserved fossil fuel will be used up in fifty years. This has brought to the attention of researchers for finding the replacement for fossil fuel in near future and renewable energy such as solar cell is the best choice. Therefore, the aim of this project is to increase the efficiency of Dye-sensitised Solar Cell (DSSC) by studying the effect of different electrolytes and additives have on its performance. By comparing ACN and MPN, MPN is more stable but lower in efficiency due to higher iodine contains. The efficiency of DSSC using quasi-solid MPN is lower than that of liquid MPN due to the poor contact of the solid-state charge transport material with the dye-coated TiO_2 surface. The addition of Guanidium Thiocyanate (GuSCN) in electrolyte suppresses the recombination rate of DSSC, hence increase the V_{oc}. Similar result is observed with 4-tert-butylpyridine (TBP). TBP tends to shift the Fermi level of TiO_2 negatively and hence increases the V_{oc}. At the same time, the driving force of the electron injection from LUMO to the conduction band of TiO_2 reduced, hence, J_{sc} decreases.

TABLE OF CONTENTS

LIST OF TABLES

LIST OF FIGURES

LIST OF SYMBOLS / ABBREVIATIONS

I_{sc}	short circuit current, mA
J_{sc}	short circuit current density, mA cm^{-2}
V_{oc}	open circuit voltage, mV
V_{max}	maximum voltage, mV
I_{max}	maximum current, mA
P_{max}	maximum power, µW
η	efficiency, %
FF	fill factor
E_{bg}	bandgap energy, eV

CB	Conduction Band
DSSC	Dye-Sensitised Solar Cell
EBSD	Electron Backscatter Diffraction
EDX	Energy-dispersive X-ray Spectroscopy
EIS	Electrochemical Impedance Spectroscopy
IL	Ionic Liquid
IPCE	Incident Photon-to-current Conversion Efficiency
HOMO	Highest Occupied Molecular Orbital
LUMO	Lowest Unoccupied Molecular Orbital
MLCT	Metal to Ligand Charge Transfer
SEM	Scanning Electron Microscope
TEM	Transmission Electron Microscopy
TPGE	Thermoplastic Gel Electrolyte
TSGE	Thermosetting Gel Electrolyte
VB	Valance Band
XRD	X-ray Diffraction

ACN	acetonitrile
BMI·BF_4	1-butyl-3-methylimidazolium tetrafluoroborate

Co	cobalt
FTO	fluorine-doped tin oxide
I_2	iodide
ITO	tin-doped indium oxide
GuSCN	guanidinium thiococynate
MPN	methoxypropionitrile
$MPTiO_2$	mesoporous titanium oxide
NBB	1- butyl-1H-benzimidazole
NMP	N-methyl-2-pyrrolidone
PAA-PEG	polyacrylic acid-polyethylene glycol
PMII	1M 1-propyl-3-methylimidazolium iodide
PMMA	poly(methyl methacrylate)
PVdF-HFP	Poly(vinylidenrflouride-co-hexaflouropropylene
Ru	ruthenium
TBP	tert-bytylpuridin
TiO_2	titanium oxide

LIST OF APPENDICES

CHAPTER 1

INTRODUCTION

1.1 Background

The availability of energy sources has a great impact on the quality of human life. In current world, energy consumption already excess 400 exajoule. With increase in world population and the rising of energy demand in developing countries, the world energy consumption is expected to further augment. Besides, it also enhances the depletion of fossil fuel reserve and lead to exacerbation of the environmental pollution. Disastrous environmental pollution arising from all too frequent oil spills and climatic consequence of the green house effect caused by the combustion of fossil fuels has heightened public concern. If renewable energy resources cannot be provided in near future, quality of human life is threatened (Grätzel, 2005).

There are several alternative energy sources have been developed including those related to health and environmental concerns (air pollution and carbon dioxide emission), as well as economical and political perspectives. After concerning all these aspects, solar energy can be considered as the most important energy source. This is due to the facts that solar energy is abundant, clean, safe, and allows energy generation in remote areas. The idea of converting sun light to electric power has obsessed human being for many centuries. Our dream is to capture the energy that is freely available from sunlight and turn it into electricity which is the valuable and strategically important asset. Recently, although the efficiency of the solar power is

low, however it is a starting point toward our dream. Researches which are continuously carry out currently or in future will make our dream come true.

1.2 Basic Concept of Dye-Sensitised Solar Cell

By applying the concept form green plants (photosynthesis), solar energy conversion and storage can be achieved by photo-electrochemical processes. When sunlight or electrical lightening present, the illumination leads to excitation of the dye to an electronically excited state. The excited dye is then quenched by electron-transfer to conduction band (CB) of the semiconductor, leaving the dye in an oxidized state. The electrons in the CB are collected and flow through the external circuit to arrive at the counter-electrode. The oxidized dye is reduced by the electron donor present in the electrolyte which usually an organic solvent containing redox system, such as the iodide/triiodide couple. The reverse reaction of the redox mediator (iodide) is cause by reduction of triiodide at the counter-electrode. The voltage produced depends on the different between the Fermi level of the electron in the solid and the redox potential of the electrolyte (Longo & Paoli, 2003).

Efficiency of direct energy conversion relies on the semiconductor used. Semiconductor is the material which can absorb a fraction of the solar spectrum depending on its bandgap energy (E_{bg}). However, due to destructive hole-base reaction, many materials with adequate bandgaps are prone to photocorrosion. Furthermore, semiconductors (eg. TiO_2 and SnO_2) which are less susceptible to photocorrosion exhibit a large bandgap to permit significant collection of visible light. Surface modification with visible-light absorbing dye molecules is an alternative to overcome the limited spectral sensitivity of the wide band-gap semiconductors which are restricted to UV light. The technique of semiconductor sensitization using dye was found during development of photography in century old and progressed considerably after nineteen seventies with the advances in the development of dye sensitizers, especially Ru bipyridyl complexes with anchoring

groups to attach them to the semiconductor surface. More recently, it is applied in solar energy conversion (Longo & Paoli, 2003).

1.3 Advantages, Drawbacks and Applications

DSSC has the efficiency of 11% and this has makes it attractive as a replacement for existing technologies in "low density" application like rooftop solar collectors. Besides, mechanical robustness and light weight of glass-less collector is a major advantage. However, they may not be suitable for large-scale deployments where higher cost higher efficiency cells are often used. They might suitable for some of these roles even with small increase in the DSSC conversion efficiency (U.S. Department of Energy Office of Basic Energy Science, 2005).

In traditional cell, the electron is "promoted" within the original crystal. This will lead to low production rates. The high-energy electron in the silicon could re-combine with its own hole while producing photon and resulting no current generation. Besides, it is quite easy for an electron generated in another molecule to hit a hole left behind in a previous photoexcitation. For DSSC, the process of injecting an electron directly into TiO_2 is qualitatively different from traditional cell. The process of injection does not introduce a hole in the TiO_2, only extra electron. In this process, there is also some possibility that the electron will recombine back to the dye, but the rate at which occurs is quite slow compare to the rate that dye regains an electron from the surrounding electrolyte and electron transfer from the platinum coated electrode to species in the electrolyte is necessarily very fast (Krüger, 2003).

In comparison with traditional cells, DSSC can even work in low-light conditions, thus it is able to work under cloudy skies and non-direct sunlight. While for traditional cells, it would suffer a "cutout" at some lower limit of illumination, which cause low charge mobility and recombination will becomes a major issues.

For indoor application, such as collecting energy for small devices from the light in the house, the cutoff will be very low as well (Petch, 2004).

A practical advantage which share by DSSC and most of the thin-film technologies is the cell's mechanical robustness which leads to higher efficiency in higher temperature indirectly. Due to unstable of the traditional silicon cells, they are normally encasing in a glass box similar to greenhouse with a metal backing for strength. As temperature increase, this system suffers from decreasing in efficiency as the cells heat up internally. When same condition applies to DSSC, it was able to operate at lower internal temperature due to its structure. DSSC are normally built with only a thin layer of conducting plastic on the front layer, this allow them to radiate away heat much easier.

The main drawback for DSSC is the liquid electrolyte used. This proposes a temperature stability problem. For example, at low temperature, the electrolyte will freeze and resulted in ending production and potentially causing physical damage. While in high temperature application, the liquid will expand and making the panels sealing a serious problem. Another disadvantage is the solution of electrolyte solution. It contains volatile organic solvents and must be carefully sealed. Due to leakage and the fact that solvents permeate plastics, large-scale outdoor application and integration into flexible structure have precluded (ScienceDaily, 2008).

1.4 Aim and Objectives

The aim of this thesis is to increase the efficiency of DSSC by alter the materials used in the solar cell.

The objectives of this project are shown below:

1. To study the effect of additives in the electrolyte have on the performance of DSSC.
2. To study the effect of solvent of electrolyte has on the performance of DSSC.

By increase the efficiency, we hope that fossil fuel will be replaced solar cell in the near future so that our precious environment can be protected.

1.5 Thesis Outline

This report is subdivided into 5 different chapters, generally:

1. Chapter 1
   In this chapter, background of DSSC will be introduced and the aims and objectives are described.

2. Chapter 2
   This chapter describe in detail about the DSSC and factors that will affect its performance. Literatures on the TiO_2 DSSC are reported.

3. Chapter 3
   In this chapter, the experiment methods and equipment used in this work are discussed. Furthermore, the materials used for fabrication of DSSC as well as the procedure used will be presents.

4. Chapter 4
   This chapter included the result of the FYP, which included DSSC characterisation through SEM, XRD and IV test. The results will then be analyzed and discussed further in detail by comparing with the results obtained by other researchers.

5. Chapter 5
   The last chapter will gives the conclusion to this FYP and provides recommendations for future work.

CHAPTER 2

LITERATURE REVIEW

Characteristics of metal oxides, dyes and electrolytes are essential to determine the conversion efficiency of DSSC. Therefore, in this chapter, effect of metal oxides, dyes, and electrolytes on performance of DSSC will be discussed in detail. In section 2.2, single-, double- and multilayer oxides, and the effect of various sizes and thickness of metal oxides on DSSC efficiency will be discussed. Section 2.3 covered the effect of different dyes, such as Ru complex, and bilayer dye on DSSC performance. While in section 2.4, characteristics of liquid and quasi-solid electrolyte will be discussed. Besides, the effect of additives in the electrolyte will be considered.

2.1 Scheme of Dynamics for Dye-Sensitised Solar Cell

In earlier state of photo-electrochemical cells development, only single crystals or flat electrodes of polycrystalline films of SnO_2 (tin oxide) or TiO_2 (titanium oxide) were used. However, the light harvesting efficiency was extremely small and the efficiencies of the solar cells were lesser than 1%. The efficiency was enhanced at the beginning of nineteen nineties, in Lausanne, Switzerland, in the laboratories of Grätzel with replacing the planar semiconductor electrode with a porous film of nanocrystalline TiO_2 particles deposited onto a conducting glass electrode. The light harvesting efficiency and the overall efficiency for solar energy conversion increased

by an order of magnitude (around 10%) attributable to the huge surface area of the nanocrystalline TiO_2 film. A schematic representation of a nonacrystalline dye sensitised TiO_2 solar cell is depicted in Figure 2.1.

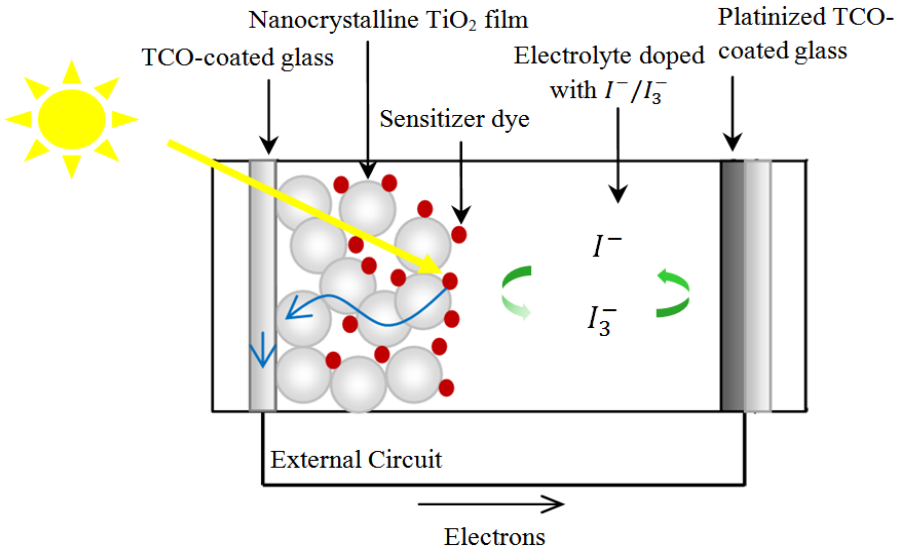

Figure 2.1: Representation of a dye-sensitised TiO_2 solar cell

$TiO_2\|S + hv \rightarrow TiO_2\|S^*$	excitation	(2.1)
$TiO_2\|S^* \rightarrow TiO_2\|S^+ + e_{cb}$	injection	(2.2)
$TiO_2\|S^+ + e_{cb} \rightarrow TiO_2\|S$	recombination	(2.3)
$TiO_2\|S^+ + 3/2\ I^- \rightarrow TiO_2\|S + 1/2\ I_3^-$	relaxation	(2.4)
$1/2\ I_3^- + e_{(pt)} \rightarrow 3/2\ I^-$	regeneration of dye	(2.5)
$I_3^- + 2e_{cb} \rightarrow 3I^-$	dark current	(2.6)

The relative energy levels and the kinetics of electron transfer processes at the liquid junction of the sensitised semiconductor | electrolyte interface determine the efficiency of a DSSC in the energy conversion process. For efficient operation of the solar cell, there are few criteria must be fulfilled. The criteria are listed as below.

1. The electron injection must be faster than the decay of the dye excited state.
2. Rate of re-reduction of the oxidized sensitizer (dye cation) by the electron donor in the electrolyte (Equation 2.4) must be higher than the rate of back reactions. Back reactions included the reaction of the injected electrons with

the dye cation (Equation 2.3) and reaction of injected electrons with electron acceptor in the electrolyte (Equation 2.6).

3. The kinetics of the reaction at the counter-electrode must also guarantee the fast regeneration of charge mediator (Equation 2.5) otherwise this reaction could become rate limiting in the overall cell performance.

For DSSC consisted of nanocrystalline TiO_2 and Ru bipyridyl complexes (dye), it has fast charge injection process which usually in femtosecond time domain. In contrast, the electron back reaction (Equation 2.3) is much slower, usually in several microseconds or longer. The difference in these 2 processes (forward and reverse electron transfer rate) allows the efficient processing of the reduction of the dye cation by iodide and the percolation of the injected electrons in the TiO_2 film to arrive at the back contact (counter-electrode).

The dye regeneration rate reaction which represented by Equation 2.4 is essential for the efficient of the cell since it affects the relative amount of electrons that leave the semiconductor and contribute to photocurrent. Base on some experiment, there are suggestion regarding the mechanism for of re-reduction of the oxidized dye by iodide. They proposed that, re-reduction of the oxidized dye involves the formation of I_2 radial on the surface of the oxide and then followed by disproportion. The reaction can be represented by Equation 2.7 and 2.8.

$$TiO_2|S^+ + 2I^- \rightarrow TiO_2|S + I_2^{*-} \quad (2.7)$$

$$2I_2^{*-} \rightarrow I^- + I_3^- \quad (2.8)$$

Depends on the nature and concentration of the cation in electrolyte, this pathway can be preferred if iodide ions were adsorbed on the surface. For the injected electrode, besides dye cation, it will also react with triiodide (Equation 2.6). This reaction (“dark current”) is the main loss mechanism for the DSSC and it might happen by means of traps and intermediate reactions (Longo & Paoli, 2003).

2.2 Metal Oxides – Nanocrystalline Titanium Oxide

When choosing semiconductor for DSSC application, there are few factors which must be considered. First requirement related to the relative energy levels at the semiconductor | sensitizer interface. The CB (conduction band) edge of the semiconductor must in the location which allows charge injection from the exited-state of the dye. Secondly, morphological and structural characteristics of the semiconductor film must be considered as its play a very important role in the processes for the solar cell operation. This is due to the fact that semiconductor nanoparticles exhibit a large number of traps (band gap localized states) and it can present distinct Fermi Levels. This will definitely affect the kinetics for charge transfer and recombination at the semiconductor | sensitizer interface. Besides, a suitable degree of porosity is also an important factor. The structure of the pores must guarantee the regeneration of the oxidized dye by permit the penetration of the electrolyte containing the redox couple, and permit an effective mass transport of electroactive species by diffusion. Moreover, the interconnected particles must exhibit in the porous film to allow the percolation of injected electrons. Fifth factor is regarding the crystallinity of the particles as it tends to influence the injection of electron and their transport through the network of particles in the film. Lastly, the thickness of the film must be well design since increasing the film thickness also increase the probability for dark current which is main loss mechanism in a nanocrystalline TiO_2 DSSC (Equation 2.6). There is an optimal TiO_2 film thickness in which the cell produces the maximum photocurrent.

Besides factors that mentioned, the characteristic of the transparent electrode used as substrate will also affect the properties of porous TiO_2 films. Usually, glass electrodes are coated with a thin conductive layer of fluorine-doped tin oxide (FTO) or tin-doped indium oxide (ITO). These electrodes have sheet resistivity of 10-20 Ωcm^2 and it is quite transparent in the visible region. However, as glass-ITO electrons undergo heat treatment, electrodes resistivity can increase considerably which cause an increase in the series resistance, decrease DSSC performance. When glass-FTO electrons are heated to the same temperature as glass-ITO electrons, this

effect is not observed. Therefore, transparent based on FTO are more adequate for the application in DSSC than ITO electrodes.

Compare to cells prepared by tin oxide (SnO_2) and zinc oxide (ZnO), cells prepared with TiO_2 in anatase crystalline form exhibit higher performance. TiO_2 is a wide bandgap semiconductor ($E_{bg} \sim 3.2eV$), non-toxic and inert compound, an inexpensive and readily available material (Longo & Paoli, 2003).

2.2.1 Effect of Grain Size, Number of Layer and Thickness

Size of TiO_2 tends to affect the efficiency of the DSSC. Hence, the characteristics of DSSC with single layer TiO_2 with different sizes were studied. This aspect has studied by Ngamsinlapasathian, Sreethawong, Suzuki and Yoshikawa in year 2004. In their study, cells are made from nanocrystalline mesoporous TiO_2 with grain size of 10 to 15 nm (MP-TiO_2) and commercial P25 titania with grain size of 30 to 60 nm.

Their results show that, cell with MP-TiO_2 has much higher short-circuit photocurrent density (J_{sc}) than P25 cell. Furthermore, it also has higher incident photon-to-current conversion efficiency (IPCE) in the region between 400 and 475nm. This is due to its anatase phase, high surface area, and mesoporous structure. On the other hand, IPCE is lower in red region compare to thick P25, and when thickness increases, J_{sc} decreases noticeably.

Nanoparticles TiO_2 is able to increase the area of TiO_2 film and propose IPCE than large particles. However it was unable to absorb red light through light scattering due to insufficient film thickness. Besides, although thick TiO_2 film are preferable to support large amount of dye to obtaining higher cell performance, thick film tends to crack because of film shrinkage, increases tendency for recombination between electrons injected from the excited dye to conduction band of TiO_2 and I_3^- ion in the electrolyte, and hence, reduces efficiency. Therefore combination of various size of TiO_2 is recommended as nanoparticles are essential for increase

surface area, and hence, amount of dye, while large particles (scattering particles) are needed to enhance absorption of red light and prevent film shrinkage. It is impracticable to increase surface area and light scattering due to their inversely proportional relationship. For all researches mentioned below, N719 is used as dye.

In 2008, a study proposes the relationship between size of scattering particles and the corresponding efficiency. The main nano-TiO_2 layer is anatase particle with 20nm diameter. Thickness of the main-layer is 7 µm (1L) and 14 µm (2L) respectively. The scattering rutile TiO_2 particles consist of particles size of 0.3 µm (G1) and 0.5 µm (G2). The efficiency (η) for 1L, 1L+G1, 1L+G2, 2L, 2L+G1 and 2L+G2 are 7.55%, 8.94%, 8.78%, 8.60%, 9.09% and 9.15%. Similar with research done by Z. S. Wang et al., their result show that, smaller scattering particles exhibit better scattering efficiency then large scattering particles. However, this is only applicable to main layer with thickness of 7 µm. For main layer with thickness of 14 µm, there is no significant size-dependent scattering efficiency due to reduced quantity of transmitted light (Koo et al., 2008).

The thick film can also be fabricated by blend MP-TiO_2 with P25 (MP-TiO_2 + P25). The P25 is able to increase the thickness and hence, lead to higher absorbed in red region. The IPCE around 70% was achieved at wavelength of 530nm. Besides, it converts incident light to current efficiently in the region from 400 to 750 nm. Furthermore, it also helps to prevent film cracking. However, the photocurrent was not high enough to get high cell efficiency. Ngamsinlapasathian et al. (2004) discovered that, cell performance can be improved by using double-layered MP TiO_2/P25 TiO_2 electrode. In their research, single layer electrode consists of MP-TiO_2 + P25. Double layer cell consists of MP-TiO_2 + P25 as top layer, transparent MP-TiO_2 layer as intermediate layer and substrate. They concluded that, double layer cell has higher dye absorption due to high surface area of MP-TiO_2 (double layer cell has more MP-TiO_2). Besides, it also able to increase light scattering and lead to greater light harvesting efficiency. Solar conversion efficiency up to 8.1% was obtained for double layer cell.

In May 2004, Z. S. Wang et al. found that, multilayer structure is superior to the mono- and double-layer structure. In their research, TiO_2 photoelectrodes with seven different structures was design and investigated. There are four types of paste used. Firstly, paste N with 100 wt% 23nm TiO_2 nanoparticles. Secondly, paste M' which consists of 60 wt% 23nm TiO_2 nanoparticles and 40 wt% 50nm TiO_2 nanoparticles. Thirdly, paste M which consists of 60 wt% 23nm TiO_2 nanoparticles and 40 wt% 100nm TiO_2 nanoparticles. Lastly, paste S with 100 wt% 100nm TiO_2 nanoparticles. The structure types are N, M, NS, NM, NMS, NM'MS and NM'MS with anti-reflection layer.

For solar cell with N and M paste, M has higher efficiency. Efficiency for N and M are 7.62% and 8.37% respectively. By comparing these structures, it is clear that a suitable combination of nanoparticles and scattering particles is necessary to improve cell performance. However, it was not able to reach maximum as it subjected to back-scattering which is due to the large particles near the conducting glass results unavoidably in light loss. The back-scattering effect can be reduces or suppress by double layer film (NS and NM). Efficiency for NS and NM are 8.95% and 9.22% respectively. NM has higher efficiency due to increase in amount of small particles and resulted in increase of dye absorption. As compare to monolayer, double layer is better in term of back-scattering suppression, but above 620 nm, its light-scattering effect is not as efficient as structure M. A better result should be obtained when scattering centres are gradually increased since the path-depth length of light increases with wavelength. As a result, multilayer structure was developed. DSSC with structure of NM'MS yielded a higher efficiency than NMS, which is 9.81%. This is due to its large surface concentration of dye and the suitable light-scattering centre gradient. When a thin layer of anti-reflection layer is added, the greatest efficiency is obtained. Efficiency for NM'MS with anti-reflection layer is 10.23%.

Wang, Kawauchi, Kashima, and Arakawa (2004) proposed that, the optimal thickness of TiO_2 nanoparticles fall in the range of 15-18μm. Base on their study, the dye build up dominates the photocurrent generation below 18 μm and resulting in an increase in J_{sc}. when the thickness is more than 18 μm, recombination plays a key

role in the performance. In contrast to J_{sc}, V_{oc} decrease linearly with increase in film thickness due to charge recombination and mass transport limitation in the thinker film. Furthermore, when thickness increases, series resistance grows quickly. The redox species and electrons migrate in a long path length to complete the circuit are the key factor that lead to increase in series resistance. By taking into account of both J_{sc} and V_{oc}, the efficiency of solar cell increase with thickness until 16 µm and follow by reduction.

2.2.2 Effect of Anatase and Rutile Phase

Microstructure of metal oxides (main layer) is believed to affect the conversion efficiency of DSSC. This was proven Ngamsinlapasathian et al. Their result shows anatase phase is essential for main layer of the metal oxide. This is partly due to the difference in the flat-band potential of anatase and rutile as the anatase conduction band is 0.2 V more negative than rutile. Therefore, if the same redox mediator is employed, a larger maximum photovoltage can be obtained on anatase than on rutile. Besides, short-circuit photocurrent of rutile is 30% lower than anatase due to lesser amount of adsorded dye as a result of smaller surface area per unit volume compared with the anatase (G. H. Li et al., 2009).

For scattering particles, the different in refractive index between anatase and rutile scattering particles tend to influence the scattering efficiency. Hence, the effects of crystal phase of scattering particles on photovoltaic performance are investigated. Ultraviolet-visible spectroscopy (UV-Vis) reflectance spectra show that, rutile scattering particle has higher reflectance than anatase in almost the whole wavelength region. This causes slightly higher J_{sc} for rutile scattering particle film than for anatase scattering particle film. Thus, rutile particles-based scattering layer has better scattering efficiency compare to anatase-base scattering layer (Koo et al., 2008).

2.2.3 Sintering Time and Temperature

One of factors that affect the DSSC's efficiency is the sintering temperature. Ngamsinlapasathian et al. (2004) found that, the high efficiency was obtained when the cell sintered at 500˚C for 1h (single layer) and 450˚C for 2h (double layer). The result obtained shows that, further increase in J_{sc} was noticed when the sintering temperature was increased. This is because increase in sintering temperature tends to result in better crystallinity which is favourable for anchoring the geometry of the dye and hence leading to faster electron transport. However, the longer the sintering time at high temperature was, the more the resistivity of conducting glass. The increase in resistivity caused series resistance in the cell increases and thus the V_{oc} and *FF* reduce. Therefore, the electrodes should be sintered at optimum sintering temperature to obtain high J_{sc} due to higher crystallinity and complete elimination of the organic surfactant in the pores. At the same time, the cell should sinter at optimum sintering time to minimize resistivity.

2.3 Dye Sensitizer

The dye sensitizer is acting as molecular electron pump in the DSSC. It is function by absorbs the visible light, follow by pump an electron into semiconductor and then accepts electron from the redox couple in the electrolyte. This is a repeat cycle. In order to be suit for DSSC application, the dye must present in certain characteristics to ensure efficiency in the charge injection and regeneration process. Firstly, it must have a strong absorption in the visible range. Secondly, it must have high stability and reversibility in the oxidized, ground and excited states. Lastly, it must also have a suitable redox potential in relation to the semiconductor conduction band edge and redox charge mediator in the electrolyte. In this section, characteristics of Ru Complex dye will be discussed (Longo & Paoli, 2003).

2.3.1 Single Layer Ru Complex

The dye sensitizer is acting as molecular electron pump in the DSSC. It is function by absorbs the visible light, follow by pump an electron into semiconductor and then accepts an electron from the redox couple in the electrolyte. This is a repeat cycle. In order to be suit for DSSC application, the dye must present in certain characteristics as listed in below to ensure efficiency in the charge injection and regeneration process (Longo & Paoli, 2003).

1. It must has a strong absorption in the visible range.
2. It must has high stability and reversibility in the oxidized, ground and excited states
3. A suitable redox potential in relation to the semiconductor conduction band edge and redox charge mediator in the electrolyte

The most efficient sensitizers are based on bipyridyl complexes of transition metals, mainly ruthenium (Ru) (II). This is because generally Ru complexes show a strong and broad absorption band in the visible range due to metal to ligand charge transfer (MLCT) leading to excited states with long lifetimes. Besides, oxidized Ru(II) complex has long-term chemical stability. Using amphidentate ligands, for example, CN- or -SCN, chelation of the metal which will lead to some tuning of spectral response can take place. By altering peripheral groups (axial ligand or chain substitution), the tendency of the dye to aggregate on solution or on the surface can be affected. Additionally, the choice of anchoring groups of the dye also has a curial effect in the performance of the DSSC. Normally, the bipyridyl rings with anchoring substituent groups at 4,4’-positions are employed in order to ensure the molecular organization of the dye on the oxide surface, as well as to promote electronic coupling of the donor levels of the dye with the acceptor levels of the semiconductor. Carboxylic or phosphonic acids are the preferred anchoring groups for dye used in solar cells because they react spontaneously with the surface hydroxylic group of the oxide surface to form the corresponding esters which is the linkages that exhibit good stability. Last but not least, the selection of counterions and the degree of protonation which are related to the solubility of the dye in organic or aqueous solvents are also

included in the molecular design of the photosensitizers. Numerous research groups started to tune the electronic and optical properties by exchanging one or more of the ligands with using N3 as reference. Five different approaches included substituting the chromophore of the dye, change protonation level of N3, extending the π-system, develop amphiphilic dyes with alkyl chains (two of the four carboxlic groups were replaced by long alkyl chains) and using different anchoring groups (Dye Sensitized Solar Cell, n.d.).

The efficiency for different Ru complex such as N3, N712, N719, Z910, K19, N945, K73, N621, Z907, Z955, HRS-1and Black dye is 10.0%, 8.2%, 11.2%, 10.2%, 7.0%, 9.6%, 9.0%, 9.6%, 7.3%, 8.0%, 9.5% and 10.8%. This shows that different attach group will cause variation in efficiency (Dye Sensitized Solar Cell, n.d.). The efficiency might not be the same for every research or experiment. This is because the metal oxide and electrolyte used might be different. For example, Ngamsinlapasathian et al. only achieves the efficiency of 8.1% with using N719 dye and in this journal, efficiency reach 11.2%.

2.3.2 Bilayer Ru Complex

A recent study recovered that, the efficiency of the bilayer dye DSSC has the efficiency which is summing up those with only one dye. The dyes used are black dye and NK3705. The result shows that, DSSC with using NK3705 obtained J_{sc} of 4.2mAcm^{-2}, V_{oc} of 0.62 mV, fill factor of 0.71% and efficiency of 1.85%. DSSC with using black dye obtain higher efficiency which is 7.28%. Besides, J_{sc} increases to 20.4 mA cm^{-2}. When two dyes used, highest efficiency achieved. The characteristic of two dyes DSSC included J_{sc} of 21.8 mA cm^{-2}, V_{oc} of 0.70 mV, fill factor of 0.60% and efficiency of 9.16%. Although bilayer cell has higher efficiency than single layer DSSC, its efficiency is reduced by unfavourable interaction between two dye molecules (Inakazu, Noma, Ogomi, & Hayasea, 2008).

2.4 Electrolyte

For stable operation of the DCCS, the redox couple in the electrolyte plays in importance role which it must carry the charge between the photoelectrode and the counter-electrode for dye regeneration. After the injection of electron, the oxidized dye must be reduced by the electron donor in the electrolyte as soon as possible. Therefore, the selection of charge mediator must consider its redox potential, which must be suitable for dye regeneration. Furthermore, the redox couple must be able to reverse fully and should not absorb visible light. Lastly, the solvent should permit the rapid diffusion of charge carries, at the same time, not causing desorption of the dye from oxide surface. The properties of redox couple will affect several processes in DSSC. This included re-reduction of the oxidized state of the dye, electron-transfer kinetics at the counter-electrode, dark current reaction, the process of ion-pairing with the dye and charge transport in the semiconductor film an in solution (Longo & Paoli, 2003).

Recently, under irradiation of 100mWcm^{-2} (AM 1.5), the overall light-to-electricity conversion efficiency of DSSC with liquid electrolyte have reached 11% (Yang et al., 2007). However, the achievement of long-term stability at temperature about 80 to 85˚C, which is an important requirement for outdoor application, still remains a major challenge. The critical factors limiting the long-term performance of DSSC, especially at elevated temperature are the leakage of liquid electrolyte, possible desorption of loosely attached dyes, photodegradation in the desorbed state as well as corrosion of the Pt counter by the triiodide/iodide couple (P. Wang et al., 2003).

Several attempts have been made to improve the long-term stability, which included p-type inorganic and organic hole conductors. Due to inefficient hole transport which is causes by imperfect contact between the dye-anchored electrode and hole conductor, the efficiency with using hole conductors are relatively low (Kang et al., 2004). Furthermore, as compare to liquid electrolyte, DSSC with solid polymer electrolyte achieved lower conversion efficiency due to high recombination

rate at the TiO_2/solid-state electrolyte interface and the low conductivity of solid-state electrolyte (Lu, Koeppe, Gu, & Sariciftci, 2006).

An alternative to overcome the disadvantage of hole conductors is used polymer gel to quasi-solidify the liquid electrolyte. Polymer gel is a system that consists of a polymer network swollen with a solvent. It has both cohesive properties of solid and diffusive transport properties of liquid. Polymer gel electrolytes possess a high ambient ionic conductivity but poor mechanical properties compared to pure polymer electrolytes.

The development of non-corrosive electrolyte is the direction of one current research. The most promising result is obtained with Co(II)/Co(III) redox couple with overall efficiency up to 4%. However, the researchers do not considered the obvious benefits which could be achieved. These benefits may be explained by the perfect functioning of I^-/I_3^- couple wherein negatively charged ion carries the positive electrical charge. The resulting electrostatic repulsion between the electron in the TiO_2 and the hole on the I_3^- ion may be advantages for slow interfacial recombination kinetics (Lenzmann & Kroon, 2007).

2.4.1 Liquid Electrolytes

The efficiency up to 11% have been reported in section 2.4 and this result is typical achieved with acetonitrile (ACN) based liquid electrolyte. ACN is a low-viscosity volatile solvent and this electrolyte consists of ACN:VN (3/1), 1M 1-propyl-3-methylimidazolium iodide (PMII), 0.03 M iodide (I_2) , 0.1 M guanidinium thiococynate (GuSCN) and 0.5 M tert-bytylpuridin (TBP). It uses comparatively low iodide concentration. It is able to achieve high efficiency; however, it was not able to achieving the best long term stability at the same time. Therefore, other electrolyte formulations which use less volatile solvents or ionic liquids along with higher iodine concentrations are desired (Yang et al., 2007).

An alternative for acetonitrile based liquid electrolyte is methoxypropionitrile (MPN) based liquid electrolyte. This electrolyte is referred to as robust electrolyte. It consists of MPN, 1M 1-propyl-3-methylimidazolium iodide (PMII), 0.15 M iodide (I_2), 0.1 M guanidinium thiococynate (GuSCN) and 0.5 M 1-butyl-1H-benzimidazole (NBB). MPN-based electrolyte has higher stability than ACN-based electrolyte, but it leads to a lower efficiency output which is in the range of 7% to 9%. (Lenzmann, & Kroon, 2007) Both ACN- and MPN-based liquid electrolyte are use widely due to acceptable vapour pressure which ranging from 9 hPa for MPN-based to 97 hPa for ACN- based (Dye Senitized solar cells, n.d.).

Ionic liquid electrolyte is other type of liquid electrolyte. Ionic liquid (IL) is a salt in the liquid state. The toxic organic solvents use in liquid electrolyte may be disadvantages to preparation and operation of DSSC. Organic solvents are chemical class of compounds share a common structure which is at least 1 carbon and 1 hydrogen atom. The organic solvents such as acetonitrile, methoxyacetonitrile or methoxypropionitrile are even harmful to the environment (An et al., 2006). While ordinary liquids are made up of electrically neutral molecule, ILs are composed solely of anions and cations. Cations included Imidazolium, Pyrazolium, Triazolium, Thiazolium and more. Anions are classified into organic and inorganic. The examples of organic anions are Sulfonate, Imide, and Methide. While for inorganic anions, they are BR_4^- and PR_6^-. R is represent halide, CF_3, C_2F_5, and other electron withdrawing aryl or alkyl substitutes. ILs based liquid electrolyte have several advantages, which are, non-flammable, non-corrosive, thermally and hydrolytically stable, wide liquid range and negligible vapour pressure (Covalent Associaes, Inc., n.d.). It is environmental friendly but the efficiency was low compare to ACN- and MPN- based liquid electrolyte. An example of ionic liquid is $LiI(C_2H_5OH)_4$-I_2 with efficiency of 4.9% (Xue et al., 2004).

2.4.2 Gel Electrolytes

Generally, gel electrolytes are obtained by incorporating a large amount of a liquid plasticizer and/or solvent which containing the desired ionic salts into a polymer matrix. During gelation, a dilute or more viscous polymer solution is converted into a high viscosity system, a stable gel with polymer host structure. The name "gelator" is giving for the polymer or oligomer that from this stable network because it solidifies the liquid phase. The mechanical properties of the gel can be improved by cross linking the components and/or incorporated thermoset into gel electrolyte formulation. Hence, gel can be form by either chemical or physical crosslinking process. Physical crosslinking is also known as "enlargement network". For covalent crosslinking it will leads to the irreversible formation of gels. The polymer use as polymer matrices included poly(ethylene oxide), poly(acrylonitrile), poly(vinyl pyrrolidinine), poly(vinyl chloride), poly(vinyl carbonate), poly (vinylidene fluoride) and poly(methyl methacrylate) (Günes, 2006).

Succinonitrile is a molecular plastic crystal, when silica nanoparticles and 1-butyl-3-methylimidazolium tetrafluoroborate (BMI·BF_4) added, it become gel by introducing the hydrogen bond (O-H...F) network. By adding silica nanoparticles and BMI·BF_4, the thermostability of the cell was improved. Moreover, compare with electrolyte without succinonitrile, the electrolyte with relatively high succinonitrile content has higher conductivity, ionic diffusion coefficient and cell performance. Therefore, succinonitrile-based gel electrolyte satisfies the need for both thermostability and high conductivity. Besides that, the cell which is fabricated was able to work well at high temperature (60 – 80 ˚C) and shows excellent long-time stability (Chen et al., 2007).

The second type of gel electrolyte is thermoplastic gel electrolyte (TPGE). The TPGE can be prepared by a simple and convenient protocol. It has thermoplastic character, high conductivity and long-term stability. Furthermore, by tuning the composition, its viscosity, conductivity and phase state can be controlled. Using poly(ethylene glycol) as host, propylene carbonates solvent and KI/I_2 as ionic

conductors, a DSSC with a photoelectric conversion efficiency of 7.22% was achieved (Wu et al., n.d.).

Thermosetting gel electrolyte (TSGE) which is based on polyacrylic acid-polyethylene glycol (PAA-PEG) hybrid is another type of gel electrolyte. The hybrid contained shows a unique character of superabsorbent (PAA). It can absorb large amount of liquid electrolyte and the absorbed liquid is hard to be volatilized and leaked. Therefore, it maintains the merits of liquid electrolyte used in DSSC such as high ionic conductivity, good soakage property with counter electrode and porous TiO_2. DSSC which used TSGE as electrolyte attains photocurrent efficiency of 6.10% under AM 1.5 irradiation (Wu et al., n.d.).

Lianos et al. (n.d.) proposes another type of gel electrolyte which is known as nanocomposite gel electrolytes. These materials are composed of organic and inorganic substances in nanoscale. Without any other additional aids, the inorganic sub-phase can act as gelling agent, and at the same time works simultaneously as a gluing material that holding the counter and working electrode together. While for organic sub-phase, it is made of mixture of chemical substance which provides ionic conductivity. The example of organic sub-phase is silica. The advantage for these nanocomposite gels is that it can accommodate appropriate solvents within the organic sub-phase so that ionic conductivity can be raised to acceptable level. By using these gel electrolytes, the DSSCs were able to obtain the overall efficiency exceeding 5% and stable for several months under ambient conditions.

In year 2007, Lu, Koeppe, Gunes, and Sariciftci fabricated a quasi-solid-state DSSC employing commercial glue (‘‘SuperGlues’’) as electrolyte matrix. This commercial glue consists of cyanoacrylate. The cyano groups of the cyanoacrylate can form a supramolecular complex with tetrapropylammonium cations. This reaction will immobilizes the cations and hence produce a desired anionic charge transport which is essential for a good performance of the iodide/triiodide electrolytic conductor. Cyanoacrylate quasi-solid state electrolyte is a very good laminating agent and therefore offers significant advantages in the fabrication of solar cells.

Besides, it is an ordinary and low-cost compound. Efficiency of 4% was obtained for DSSC with this electrolyte.

Poly(vinylidenrflouride-co-hexaflouropropylene) (PVdF-HFP) based gel electrolyte is one of the famous polymer gel electrolyte. Since it is a fluorinated polymer, PVdF-HFP is known to be photo-electrochemically stable even in the presence of titanium oxide and platinum nanoparticles. (Kang et al., 2004) Furthermore, when compare with poly(acrolynitrile), poly(ethylene glycol), poly(oligoethylene glycol methacrylate), poly(siloxane-co-ethylene oxide) and poly(butylacrylate), PVdF-HFP shows relatively high ionic conductivities at room temperature (Suryanarayanan, Lee, Ho, Chen, & Ho, 2007).

The last type of gel electrolyte available is poly(methyl methacrylate) based DCCS. This type of gel electrolyte use sodium iodide and iodine as source of I^-/I_3^-, PMMA as polymer host, and 1,2-propanediol carbonate and dimethyl carbonate as organic mixture solvents. PMMA based gel electrolyte possessed a good long-term stability. Under irradiation of 100 mW cm^{-2} simulated sunlight, light-to-electrical energy conversion efficiency of 4.78% was obtained (Yang et al., 2007).

2.4.3 Comparison of Liquid and Gel Electrolytes

In year 2004, Kang et al. (2004) studied the characteristic of polymer gel electrolyte containing PVdF-HFP in N-methyl-2-pyrrolidone (NMP). They concluded that, the energy conversion efficiency of this electrolyte is comparable to ACN- and MPN-based liquid electrolyte. The efficiency of PVdF-HFP gel electrolyte, ACN- and MPN- based liquid electrolyte are 2.86%, 2.91% and 2.80% respectively. They also found that, compare to NMP, PVdF-HFP is hardly soluble in both ACN and MPN.

Yang et al. (2007) reported that the efficiency of quasi-solid-state DSSC is almost equal to DSSC with a liquid electrolyte under irradiation of 100 $mWcm^{-2}$. The

polymer electrolyte used in their study is PMMA-EC/PC/DMC-NaI_2 with energy conversion efficiency of 4.78%.

P. Wang et al. (2003) demonstrated that MPN- based liquid electrolyte can be gelled by PVdF-HFP polymer without affecting the charge transport of the triiodide/iodide couple inside the polymer network. The found that, at AM 0.01, 0.1, 0.5, 1.0 and 1.5, there is no different between conversion efficiency for both liquid and quasi-solid electrolyte.

The stability of the liquid and quasi-solid electrolyte has been tested out by Yang et al. (2007). In their study, two DSSCs were fabricated using the same technology. After 5 days, the efficiency for DSSC with liquid electrolyte decrease 40%, while for DSSC with polymer gel electrolyte, only 8% of decrease in efficiency is reported. After 40 days, the DSSC with liquid electrolyte only have 27% of original light-to-electrical energy conversion efficiency. For DSSC with polymer gel electrolyte, it keeps 83% of the original efficiency.

The polymer gel electrolyte is in quasi-liquid form when it is in room temperature. When the temperature increases up to 80˚C, it will become viscous liquid. When N719 is used as sensitizer, the overall efficiency is decreased approximately 35% during the first week (80˚C). This clearly reflects of the molecular structure of the sensitizer of the sensitizer on the stability of DSSC. For N719 dye, one of the 4,4'-dicarboxylic acid-2, 2'-bipyridines is replaced with 4,4'-dinonyl-2,2'-bipyridine to make the dye more hydrophobic. P. Wang et al. (2003) believes that desorption of N719 at high temperature is the factor that result in the poor thermostability of the DSSC.

2.5 Counter Electrode

There are 3 requirements for a material to be used as counter-electrode in a DSSC. Firstly, the material must has low charge-transfer resistance. Secondly, it must has

high exchange current densities for the reduction of the oxidized from of the charge mediator (Equation 2.5). Lastly, when contact with electrolyte medium use in the cell, such material must presents chemical stability (Longo & Paoli, 2003).

Up to year 2003, the best charge mediator for the DSSC is the I^-/I_3^- redox couple. Nonetheless, in several materials, the iodine reduction reaction is not reversible, and its kinetics is solvent dependent. Besides, the electron-transfer kinetics for reduction of triiodide to iodide which occur at the surface of transparent glass-ITO or glass-FTO electrodes is very slow. Platinum, particularly a thin film deposited by thermal oxidation of hexachloroplatinate is the best material that acts as catalyst and provides high exchange current for this reaction (Longo & Paoli, 2003).

2.6 Alternative Device Approaches

2.6.1 Natural Dye

Recently, although high efficiency cell have been achieved with nanoporous TiO_2 electrodes which sensitised with ruthenium complexes, there still remains the need for alternative photosensitizers. This is because ruthenium complexes are a high cost material and it has a long-term unavailability. Besides, it also required time consuming chromatographic purification procedures. In this context, application of natural dyes has numerous advantages over rare metal complexes and other organic dyes. Natural dyes have wide availability, easy extraction, can be applied without further purification, are environment-friendly and considerably reduce the cost of the devices. In natural dye, anthocyanins are a group for colour of flowers, fruits and vegetables.

In year 2007, Wongchareea, Meeyooa, & Sumaeth fabricated DSSCs using natural dye extract from rosella, blue pea and a mixture of the extracts. The efficiency is 0.37%, 0.05% and 0.15% respectively. They also found out that, extracting temperature, extracting solvent and pH of the extract solution are the

parameters which will affect the efficiency of natural dye. When the temperature decrease from 100˚C to 50˚C and pH change from 3.2 to 1.0, efficiency of rosella extract sensitised DSSC was improved from 0.37% to 0.70%. By comparing to water, after being exposed to the simulated sunlight for a short period, the efficiency of a DSSC using ethanol as extracting solvent was found to be diminished.

In year 2007, Lai, Su, Teoh, and Hon have fabricated water-based DSSC which used gold nanoparticles as a Schottky barrier on a TiO_2 electrode, commercial dyes and free natural dyes as dye sensitizer and aqueous electrolyte of $Ce4^+/3^+$ system. The function of Schottky barrier is to avoid electron from going back to oxidized dye or electrolyte. The efficiency for commercial (Crystal violet, Mercurochrome and Chlorophyll) and natural dyes [*Bongainvillea brasiliensis* Raeusch, *Garcinia suubelliptica*, *Ficus Reusa* Linn and *Rhoeo spathacea* (Sw.) Stearn.] are 0.0997%, 0.617%, 0.705%, 0.454%, 0.691%, 1.18% and 1.49%. The result shows that natural dyes have higher efficiency that commercial dye due to the carbonyl and hydroxyl groups presented on anthocyanin molecules. These groups can be bound to the surface of the TiO_2 film and hence favour the photoelectric conversion effect. While for commercial dyes, when they are aggregated or mixed together, it will lead to high thermal relation. Since absorbed energy in aggregated dyes is mostly changed into heat (loss), low efficiency resulted.

In 2008, few flowers are extracted by ethanol and HCl with pH less than 1 was added so that solution becomes deep red in colour. The oxonium ion in acidic solution results in an extended conjugation of double bonds through 3 rings of the aglycone moiety. This helps in the absorption of the protons in the visible spectra. When there is change in pH, it will tend to increase the number of conjugated double bonds in the molecules and lower the energy level of the electronic transition between the ground states and the excited state. Hence, photons absorb at greater wavelength. Due to condensation of alcoholic-bound protons with the hydroxyl groups in the surface of nanoparticles TiO_2 layer, the chemical absorption of these dyes takes place. Although natural dyes have several advantages over other organic dye and rare metal complexes, the efficiency obtain is less than 2%. In order for

natural dyes to be used in large scale photon conversion, further studies and researches are needed to improve its efficiency (Fernando & Senadeera, 2008).

2.6.2 DSSC with TiO_2 Nanotube

Recently, DSSC fabricated using order arrays of titanium oxide nanotubes which grown on titanium has been carry out. Its structure, dynamics of electron transport and recombination are the parameters which researches are interested in. When nanotubes (NT) are used as metal oxides DSSC, both interior and exterior walls are cover with dye molecules. It is able to improve the charge-collection efficiency by promoting faster transport and slower recombination. The recombination is 10 times slower than nanoparticles-base DSSC (NP) and therefore increases the charge-collection efficiency by 25%. In addition, NT-based also has higher photocurrent densities, and 20% higher light-harvesting efficiency than NP-based. However, due to the insulating oxide layer between NT which forms during anodization, its fill factor (*FF*) is lower than NP. The lower *FF* offset the gain in J_{sc} resulting the comparable performance of TiO_2 NP- and NT-based DSSC (Zhu, Neale, Miedaner, & Frank, n.d.).

CHAPTER 3

METHODOLOGY

3.1 Equipments

This chapter included characterisation techniques such as scanning electrode microscope (SEM), X-ray Diffractometer (XRD), IV tester and UV-visible spectrometer. Besides, the equipments, raw materials and apparatus used in this project are stated. Lastly, cell preparation and assembly are discussed.

3.1.1 Scanning Electron Microscope

Scanning electron microscope (SEM) is a type of electron microscope which uses a focused beam of high-energy electron to generate a variety of signals at the surface of solid specimens. When the specimen is bombarded by electrons, it emits X-ray and secondary electrons. The emitted X-ray is used in chemical analysis and secondary electrons are used for image generation.

SEM consists of column, tube and computer. The column with high voltage is connected to the filament current supply with using a tube. High voltage and current are needed for electron beam generation. With the help of the lenses the beam is focus down to a drastically narrow point which is about two nanometers across. This beam is then scanned rapidly in lines back and forth across a specimen. The electron

is excited and it is emitted by the specimen when struck with the beam. The electrons emitted provide signals to a device. This device converts electron emission to the display unit. The emitted secondary electrons are detected by electron detector and convert to a light pulse by a scintillator. The light pulse is then feed to a photomultiolier and produce a photocurrent which is amplified and projected on a display unit.

The information about the sample such as external morphology (texture), chemical composition, and crystalline structure and orientation of materials making up the sample can be revealed form the signal that derive from electron-sample interactions. The sample with the width in the range from 1 cm to 5 microns can be imaged in a scanning mode using conventional SEM techniques (the magnification is from 20X to roughly 30,000X and spatial resolution of 50 to 100nm). Besides, the analysis of selected point locations on the sample can also be performed. This approach is mainly useful in qualitatively or semi-quantitatively determining the chemical compositions of the crystalline structure by using x-ray detector (EDS), and crystal orientations by using the diffracted backscattered electrons (EBSD).

SEM is extremely important in all the fields which required characterisation of solid materials. While this contribution is most concerned with geological applications, it is important to note that these applications are a very small subset of the scientific and industrial applications that exist for this instrumentation. Compare with other microscope, most SEM are comparatively easy to operate and with user-friendly “intuitive” interfaces. Minimal sample preparation is required for many applications and data acquisition is fast. For example, less than 5 minutes per image for SEI, BSE, spot EDS analyses. Recent SEM creates data in digital formats, which are extremely portable.

The disadvantages for SEM included, samples must be solid and they must fit into the microscope chamber. There are also limitations in size. Maximum size in horizontal dimensions is usually on the order of 10 cm, and the vertical dimensions are always less than 40 mm. For most of the instruments samples, they must be stable in a vacuum in the range of 10^{-5} to 10^{-6} torr. However most samples are likely to

outgas at low pressure such as rocks saturated with hydrocarbons. Besides, “wet” samples such as coal and organic materials or swelling clays are unsuitable for examination in conventional SEM’s. Therefore, “low vacuum” and “environmental” SEMs exist so that these types of samples can be successfully examined in these specialized instruments. The EDS detectors, which is a part of SEM cannot detect very light elements such as H, He, Li, and elements with atomic numbers less than 11. Majority of SEMs used solid state x-ray detector, which known as EDS. These detectors are very fast and easy to utilize, but when compared with wavelength dispersive x-ray detectors (WDS) on most electron probe microanalyzers (EPMA), they have relatively poor energy resolution and low sensitivity to elements present in low abundances. In order for electrically insulating samples to study in conventional SEM’s, an electrically conductive coating must be applied to it. This step can only been ignore if and only if the instrument is capable of operation in a low vacuum mode.

Figure 3.1: Scanning Electron Microscope (SEM)

3.1.2 X-ray Diffractometer

Diffraction is a phenomenon occurs when wave encounters a series of regularly spaced obstacles that are able to scattering the wave. Besides, the obstacles must have spacing that is comparable in magnitude to the wavelength. The common diffraction technique included striking the monochromatic x-radiation to a powdered or polycrystalline specimen which consisting of many fine and randomly oriented particles. In order to ensure that some particles are properly oriented such that every possible set of crystallographic planes will be available for diffraction, each powder particles (or grain) must be a crystal and having a large number of them with random orientation.

The main applications of X-ray Diffractometer are to characterise the crystallographic structure and preferred orientation of the thin film. X-rays which used to provide electron beam are generated by heated tungsten filament. The chamber (also known as X-ray tube) is evacuated to prevent the oxidation of tungsten filament. The beam is accelerated toward the sample mounted on the sample stage (anode) with a potential different of 30kV. When the electron struck the sample, a spectrum of X-rays is emitted. The X-rays leave the chamber through beryllium window. Since the atomic weight of elements affects the absorption of X-rays passing through the material, beryllium is chosen as window material due to its small atomic number. Due to same reason, lead is used for shielding X-ray equipment and absorbing stray radiation. During operation, continuous cooling of anode is essential because only small portion of the energy of the incident electron beam is converted into X-ray while most of the energy is converted into heat. The heat generate could heat up the anode and anode would melt if cooling do not take place.

X-ray Diffraction (XRD) is a powerful technique used for characterizes and identifies phases. The advantages of the technique are simplification of sample preparation, rapidity of measurement, and ability to analyse mixed phases. However, it has difficulty of mounting large single crystal. Collection time is rather short even for small and weakly scattering samples since all possible crystal orientations are measured simultaneously.

Figure 3.2: X-ray Diffractometer

3.1.3 I-V Tester

I-V testing system consists of a light source, measurement electronics, computer, LCD monitor, keyboard, printer as well as the software which are needed for solar cell I-V curves measurement. The Xenon light source in I-V tester is used for illuminating test device. While for electronic load, it sweeps the cell voltage form a reverse-bias condition, through the power quadrant, and beyond open circuit voltage, V_{oc}. Data gathering, solar cell parameter calculation, printable test reports generation, and test data saving are carried out by system's computer. There are different types of solar simulators and test fixtures available, and they are selected according to testing requirements. Besides, sweep range, direction and rate are also changeable.

Basically, I-V tester used to compute solar cell parameters such as open circuit voltage V_{oc}, short circuit current I_{sc}, current density J_{sc}, maximum voltage V_{max}, maximum current I_{max}, maximum power P_{max}, efficiency and fill factor FF (Agilent Technologies, 2009). Furthermore, it also can be used for light and dark I-V

characteristics measurement. Some of the I-V tester manufacturers use irradiance monitor to compensate for lamp flicker and drift (PV Measurements, Inc., 2009).

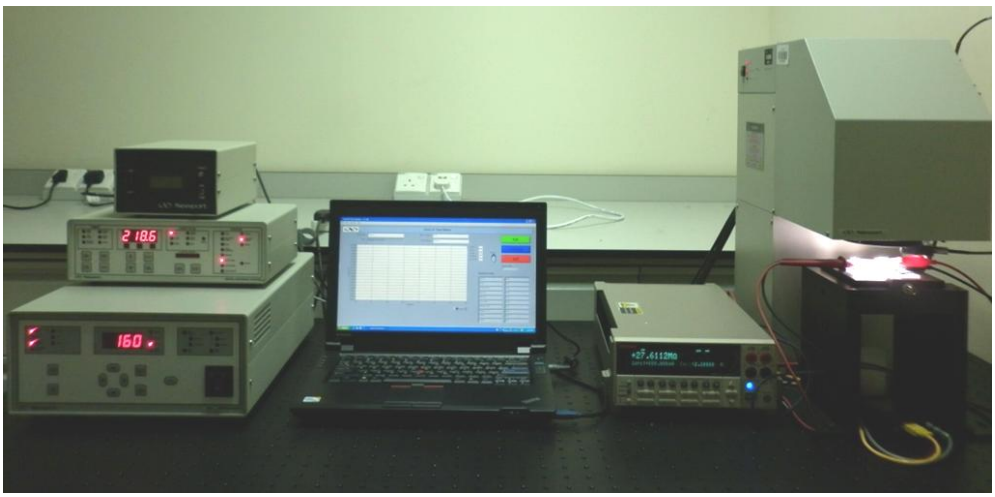

Figure 3.3: I-V Tester

3.1.4 Ultraviolet Spectroscopy

Ultraviolet Spectroscopy (UV spectroscopy) is a physical technique of the optical spectroscopy that uses light in the visible (VIS), ultraviolet and near infrared ranges. For Ultraviolet-visible spectroscopy (UV-Vis spectroscopy), its absorption spectroscopy is in the ultraviolet-visible spectral region. The perceived colour of the chemicals involved is affects by the absorption in the visible range. In this region, molecules undergo electronic transitions. Different to fluorescence spectroscopy which deals with transitions from the excited state to the ground state, UV-Vis spectroscopy measures transitions from the ground state to the excited state.

When molecules (sample) is exposed to light with an energy that matches its electronic transition, the electron is promoted to a higher orbital and some of the light energy will be absorbed. The spectrometer will then records the wavelength at which

absorption occurs and the degree of absorption at each wave length. A graph of absorbance versus wavelength is used to represent the resulting spectrum.

UV-Vis spectrophotometer is applicable in determining the absorption or transmission of ultraviolet as well as the visible light of oxide film. It measures the intensity of the light entering a sample and the light exiting a sample. The ratio of these two intensities can be expressed as transmittance (%T). The concentration of sensitising dye (absorbance) can be measure by Beer's Law which stated that the absorbance is directly proportional to the concentration of a solution. The %T is related to absorbance (A) in Equation 3.1.

$$A = 2 - [\log(\%T)] \qquad (3.1)$$

Figure 3.4: Ultraviolet Spectroscopy

3.2 Materials Used

Highly fluorine transparent conducting oxide (TCO) films coated on glass plates (FTO glass) and Pt-coated glass were the glasses that used in this project. The paste used in this project was 20nm anatase nanoparticle Titania paste. Sensitizer which was chosen for this project is Ruthenium 535-bisTBA, N719 or (cis-bis(isothiocyanato)bis(2,2'-bipyridyl-4,4'-dicarboxylato)-ruthenium(II)bis-tetrabutyl

ammonium). N719 was chosen rather than Ruthenium 535, N3 because it sensitizes metal oxide, for example, TiO_2 efficiently and giving higher open circuit voltage.

The electrolytes used were liquid ACN-based electrolyte, liquid MPN-based electrolyte and quasi-solid MPN-based electrolyte. The liquid ACN-based electrolyte was synthesized in the lab. It consists of acetonitrile, valeronitrile, 1-Butyl-3-methylimidazolium (BMII), iodine, 4-tert-butylpyridine (TBP) and guanidinium thiococynate (GuSCN). Surlyn®-30 Sealant was used to seal FTO glass and Pt-coated glass before dip into electrolyte. It is thermoplastic sealants which soften when less than 100˚C.

3.3 Fabrication Processes

FTO and platinum coated glass were cut into small pieces with using diamond cutter. The sequence of the chemical used in cleaning step for FTO glass was soap, distill water, deionized water, acetone, ethanol and lastly deionized water. For Pt-coated glass, the step was simpler. The sequence was ethanol and deionized water. Both FTO and platinum glass were dried and heated at 400˚C to remove organic solvent which contained in ethanol and acetone.

Dyes were prepared by mixing absolute ethanol with N719 and N3 powders. The concentration of dye solution used in this project was 0.3 mM. Dye solution was stored in the bottle which was wrapped with aluminium foil to avoid excitation of dye when sunlight or electrical lightening presented.

The electrolytes used were liquid ACN-based electrolyte, liquid MPN-based electrolyte and quasi-solid state electrolyte. ACN-based electrolyte was synthesized

in the lab and it is a solution of acetonitrile, valeronitrile, BMII, iodine, TBP and GuSCN.

After all the preparations were done, TiO_2 paste was applied to the conductive surface of the FTO glass by doctor blade technique as shown in Figure 3.5. By using plastic tea spoon, the TiO_2 paste was spread dripped slowly on the active area. After this, it was spread evenly on the surface of the ITO/FTO to form a layer of paste with using glass rod. The substrate was then kept in a petri disc with a piece of tissues placed underneath the glass and with few drop of ethanol dripped around the glass. It was keep for 3 min to allow the relaxation of the paste, reducing the surface irregularity. Subsequently, the substrate was dried for another 5 min at 125ºC using hotplate. The second layer of TiO_2 paste was applied using the same technique.

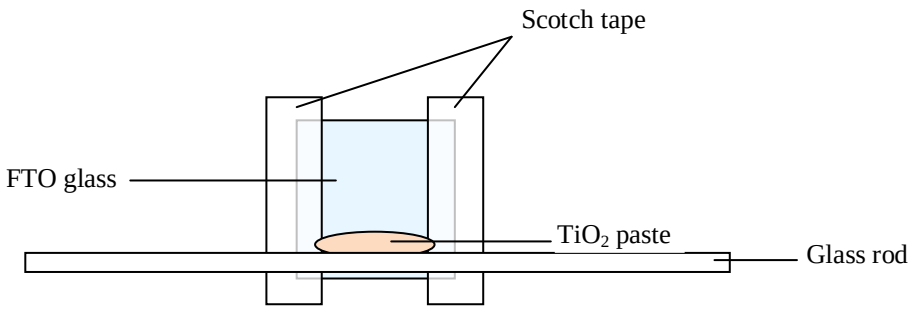

Figure 3.5: Doctor blade technique (top view)

The double layer film was annealed at 455˚C by using hot plate to remove the organic solvent. When the substrate was cooled down to room temperature, the extra paste was removed to obtain the desire area (white colour square in Figure 3.6).

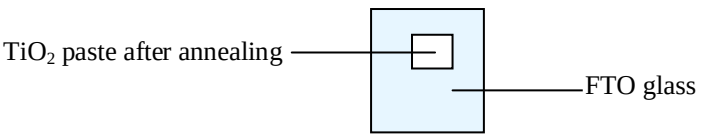

Figure 3.6: TiO_2/FTO glass which is really for next step

After this, the substrate was carefully placed into a glass bottle. N719 solution produced previously was dripped slowly into glass bottle until the substrate was fully immersed in the sensitizer. The glass bottle was placed inside a closed box at room temperature. Once TiO_2 films were immersed in dye for 24 hours, the dyed film was then taken out from the dye solution and cleaned with ethanol. Figure 3.7 (left) shows the immersion of TiO_2/FTO glass and the Figure 3.7 (right) shows the change in colour of TiO2 paste after immersion.

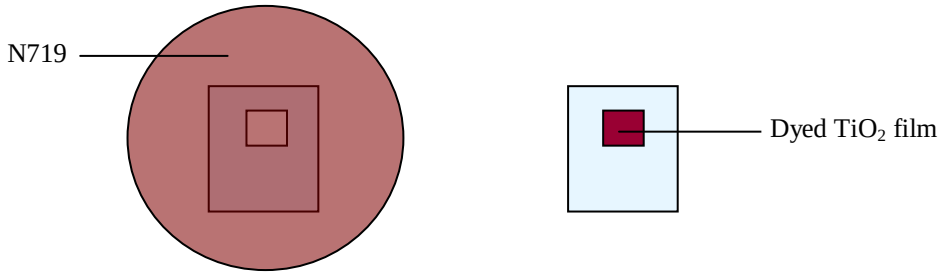

Figure 3.7: Sensitising TiO2 film with N719. Picture in the right shows the top view of the bottle.

A through hole was drill Pt-coated counter electrode. The dye-coated TiO_2 electrode and Pt-coated counter electrode were sandwiched using sealant. The cell was heated on by using hot plate to melt the sealant. As shown in Figure 3.8, weight was applied onto the cell to produce a fine seal.

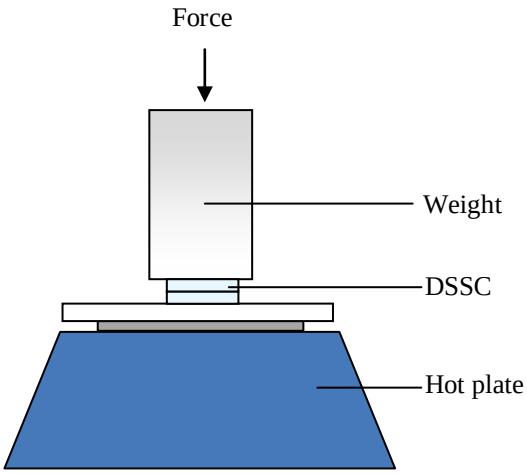

Figure 3.8: weight applied during sealing

Figure 3.9 (left) shows the introduction of electrolyte into the cell through the hole drilled with using pipette. After the electrolyte was filled, the hole was clean using a piece of tissue. This was to ensure good hole sealing.

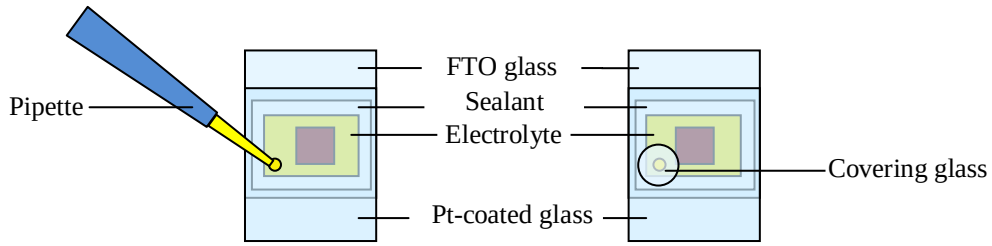

Figure 3.9: Electrolyte dripping and cell assembly.

Finally, the step followed by sealing the hole using cover glass and sealant. The completed cell is shown in Figure 3.9 (right) and it is really for testing. Flow chart for fabrication is shown in Figure 3.10.

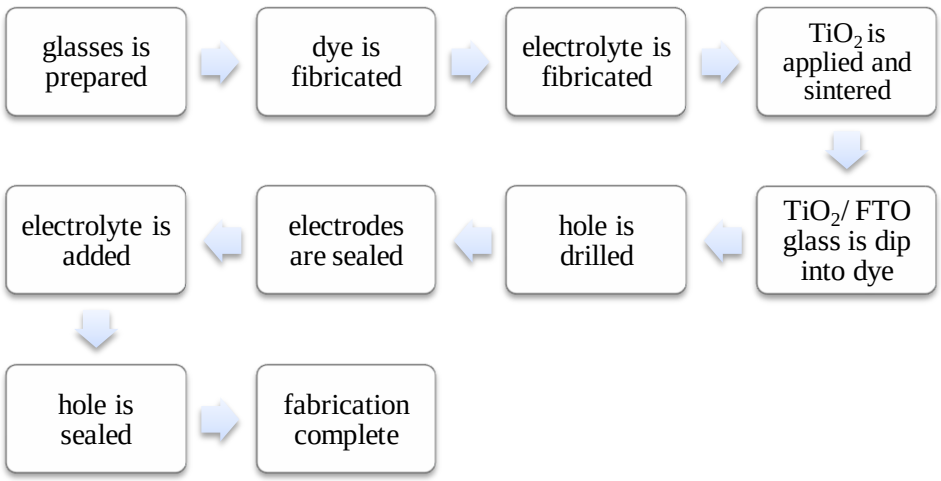

Figure 3.10: Flow chart for DSSC fabrication process

CHAPTER 4

RESULTS AND DISCUSSION

4.1 Liquid MPN-based and ACN-based Electrolyte

As discussed in chapter 2, MPN-based electrolyte uses 3-methoxypropionitrile as solvent while ACN- based electrolyte uses acetonitride and valeronitrile as solvents. When the solvents for the electrolyte are different, the additive and concentration of iodine used in the electrolyte will be affected as well hence probably will affect the efficiency of DSSC. In this section, efficiency and stability of ACN- and MPN-based electrolyte will be discussed.

4.1.1 Efficiency

The maximum energy conversion efficiency (η) of the DSSC can be calculated from Equation 4.1.

$$\eta = \frac{J_{sc}V_{oc}FF}{P} \tag{4.1}$$

where

η = conversion efficiency

J_{sc} = short circuit photocurrent density, mA/cm^2

V_{oc} = open circuit voltage, V

FF = the fill factor

P = power of the incident light, 100mWcm^{-2}

and

$$J_{sc} = \frac{I_{sc}}{A} \tag{4.2}$$

with

I_{sc} = short circult photocurrent density, mA

A = area of DSSC, cm^2

From Equation 4.1, it is clear that the efficiency is directly proportional to J_{sc}, V_{oc} and FF.

In the study of Yang & Liao (2009), DSSC that used ACN-based electrolyte should achieve higher efficiency due to higher V_{oc} and FF. This photovoltage improvement was mainly due to two factors. Firstly, the back electron transfer at the TiO_2/electrolyte interface was suppressed. Secondly, the potential where dark cathodic current started would be reduced. In the discussion onward, MPN used to represent MPN-based electrolyte and ACN representing ACN-based electrolyte.

However, in this project, different result is obtained; DSSC with MPN shows higher efficiency than that of ACN (Table 4.1). This might due to the preparation of both electrolytes was different. ACN was prepared in the laboratory with open air environment while MPN believed to be produced in an environment totally free from contaminants was purchased from a supplier in Australia. Therefore, contamination might occur during the preparation of ACN. Besides, quantity of iodine and additives required for preparation of ACN was too small and causes inaccuracy. For example, only 0.019035g of iodide was used to fabricate 20ml of ACN.

Table 4.1: Comparison of liquid MPN and ACN

	V_{oc} (V)	J_{sc} (mA/cm^2)	FF	η (%)
MPN	0.73	14.15	68.21	7.01
ACN	0.72	12.67	61.49	5.58

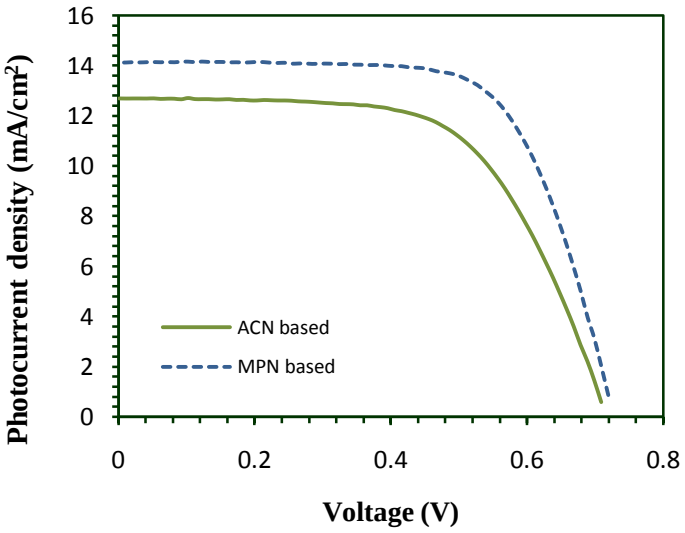

Figure 4.1: Photocurrent-voltage curve of liquid ACN and MPN

Figure 4.1 shows that, MPN exhibits higher J_{sc} compare to ACN, the associated value for MPN and ACN are 14.15 and 12.67 mA/cm^2 respectively. Yang & Liao (2009) found that the increase of J_{sc} in MPN was associated with the suppression of triiodide reduction at the TiO_2/electrolyte interface and hence, led to a facile injection of electron carriers into FTO substrate.

4.1.2 Stability

Performance of the solar cell can be affected by its stability. Low stability solar cell will degrade in short period of time and its efficiency will decrease tremendously. This is an undesirable characteristic of DSSC. No one will like to change the solar cell frequently. This will be costly and at the same time, not environmental friendly. In this study, measurement was taken once each day for the period of 32 days using a particular solar cell to determine the stability of that cell. The measurement was not able to perform continuously within these 32 days due to the lab was close during weekends.

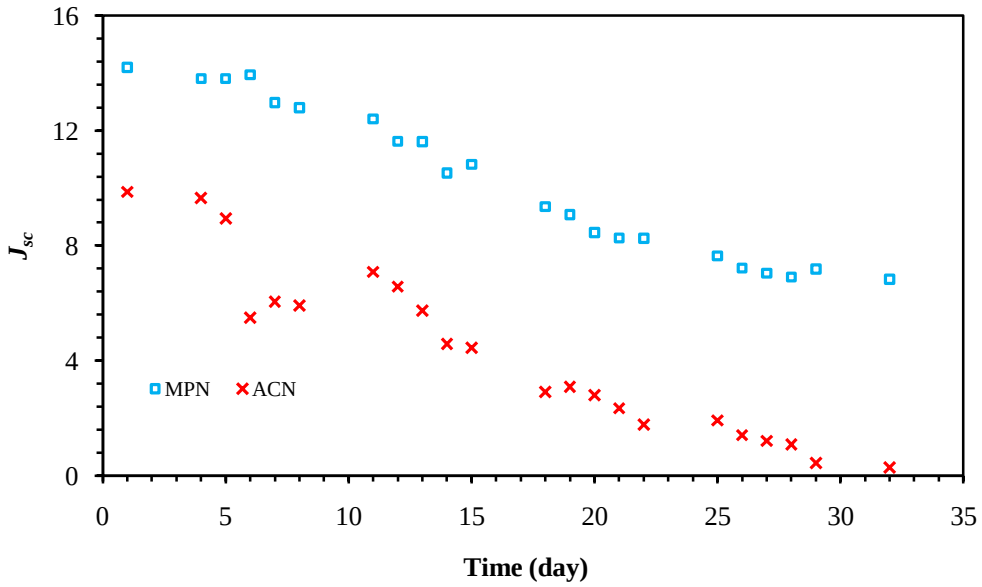

Figure 4.2: J_{sc} for ACN and MPN

Figure 4.2 shows that J_{sc} decrease with the increase of time. Both ACN and MPN decrease at a similar rate. After 32 days, J_{sc} for ACN and MPN was reduced by 7.3649 mA/cm^2 and 9.5759 mA/cm^2 respectively. Decrease in J_{sc} was suspected to be originated from the dye desorption. However, Kang et al. (2004) found that the dye desorption essentially did not occur in ACN and MPN. In his study, amount of dye desorbed from the TiO_2 firms into the contacting solvent for 4 days was measured. For comparison, NMP (N-mthyl-2-pyrrplidone), MPN and ACN were used as the solvent. By comparing to ACN and MPN, dye molecule desorbed occur NPM to some extend. This suggested that the decrease in the J_{sc} was not due to the desorption of the dye from the TiO_2 to electrolyte.

The second posibility of J_{sc} reduction is the damage of the electrolyte. Leonardi (2010) found that, the strong reduction in J_{sc} was due to the cells were damaged from the interaction with oxygen and moisture. His idea was supported by Electrochemical Impedance Spectroscopy (EIS) measurements. Based on the Nyquist diagram (Figure 4.3), the high resistance was located at the part of the curve which representing the ionic diffusion (red circle). This curve was enlarged very much toward higher resistance over a period of time. This represented the increment in diffusion resistance which was mainly due to reduction of I_3^- ions concentration. This

was evident that the component of the cell that had been damaged the most was the electrolyte.

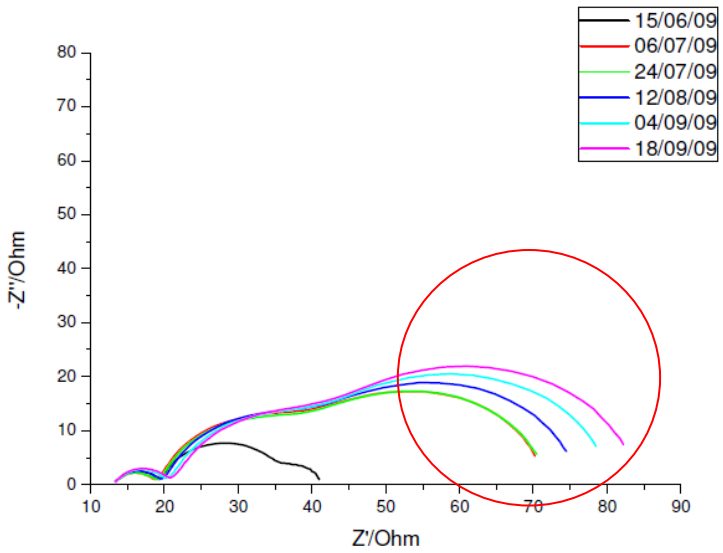

Figure 4.3: EIS measurement over a period of time – Nyquist diagram (Leonardi, 2010)

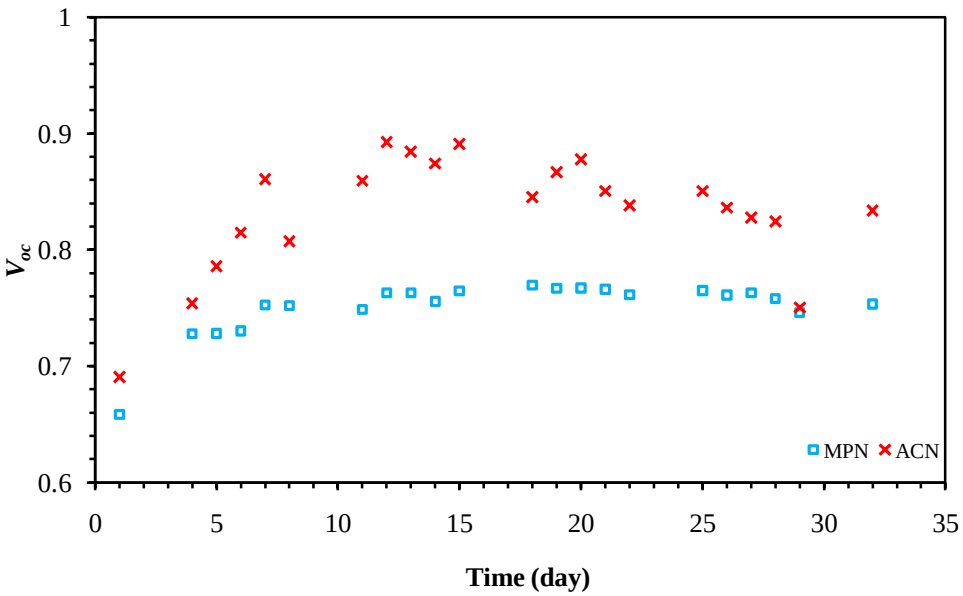

Figure 4.4: V_{oc} for ACN and MPN

Figure 4.4 shows that V_{oc} increases slowly in the beginning and become constant in the end of the day. This shows that the V_{oc} is not much affected with increasing time.

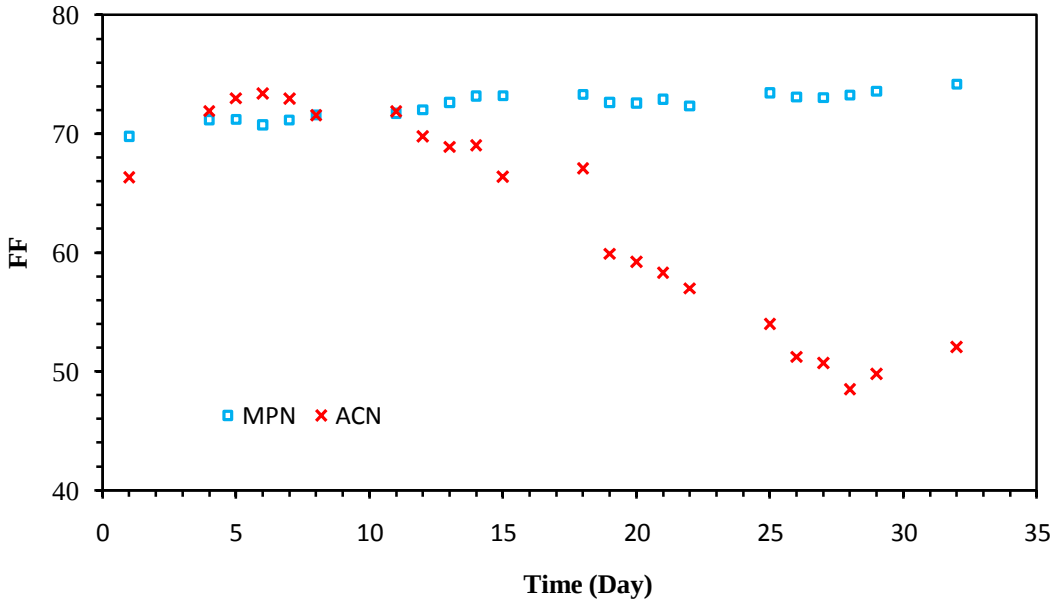

Figure 4.5: *FF* for ACN and MPN

FF is defined as the ratio of actual output ($V_{pmax} \times I_{pmax}$) to dummy power output ($V_{oc} \times I_{sc}$). It is shown in the Equation 4.3.

$$FF = \frac{V_{pmax} \times I_{pmax}}{V_{oc} \times I_{sc}} \times 100 \tag{4.3}$$

where

FF = fill factor

V_{pmax} = voltage at maximum power, V

I_{pmax} = current at maximum power, mA

V_{oc} = open circult voltage, V

I_{sc} = short circult photocurrent density, mA

This is a key parameter in detemining the perfomance of a solar cell. Typical solar cell have *FF* which is larger than 70%. As shown in Figure 4.5, the is hardly any changes in *FF* with time for MPN while for ACN, *FF* drops tremendously with the increase of time. This is probably due to the high leakage of the electrolyte from the DSSC as ACN contains a volatile solvent (acetonitride). Hence, the amount of electrolyte in the DSSC reduces and *FF* decreases. For MPN, it is a robust electroyte.

It is more stable than ACN and leakage is not a main problem, therefore, *FF* remains stable.

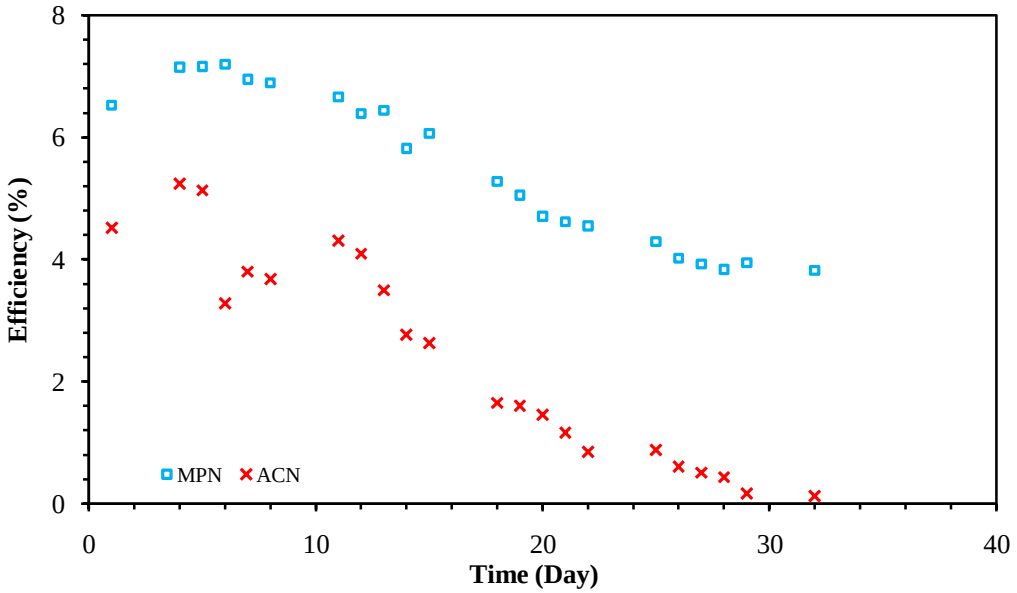

Figure 4.6: Efficiency for ACN and MPN

Figure 4.6 shows the efficiency of DSSC with ACN and MPN. The highest efficiency is recorded at day 6 and day 4 for MPN and ACN respectively. This is due to time is needed for the added electrolyte to penetrate into the TiO_2 layer (Kang et al., 2004). The efficiency will then start to decrease with time. The trend for MPN is relatively stable than ACN. The efficiency in day 32 decreases by 46.95% compare to the highest recorded efficiency while for ACN, it decreases by 97.58%. This shows that ACN is not able to achieve a long term stability compare to MPN. The phenomenon is supported by the study of Yang et al. (2007) and Lenzmann & Kroon (2007). The low stability of ACN is due to its low iodide concentration and solvent. Acetonitrile is a low-viscosity volatile solvent, easily evaporated at normal room temperature (25˚C).

Figure 4.6 also shows that the efficiency of ACN to reduce at a higher rate compares to MPN. The numeral data for both ACN and MPN are shown in appendix A, Table A and B respectively. In order to determine the factor that affects the efficiency the most, it is needed to analyse in detail the trend of each parameter

affecting the efficiency (Figure 4.2 – 4.5). J_{sc} for MPN and ACN decreases in similar rate. Therefore, it is not the primary reason that causes higher reduction rate of ACN's efficiency. ACN has higher V_{oc} than MPN, but it is not enough to compensate the decrease in *FF*. V_{oc} for the ACN is higher than MPN by 0.1 to 0.2V, however, its *FF* is lower than MPN by 0 to 20 times and decrease enormously after day 12. In conclusion, *FF* is most significant factor that affects efficiency of ACN.

Generally, the long term stability for liquid electrolyte is low. This is due to that liquid electrolyte easily volatilized and leak in long-term operation. Besides, the life-time of the DSSC will be affected by the presence of water in the solar cell from the surrounding through the imperfection packaging sealants. This will further cause decrease in life-time of photogenerated electrons on the working electrodes which induces the occurrence of the dark current to the electrolyte. Hence the life-time of the DSSC is significantly deteriorated (H. L. Lu et al., n.d.).

4.2 Liquid and Quasi-solid MPN-based Electrolyte

Table 4.2 shows that the DSSC with quasi-solid (gel) electrolyte has similar efficiency to that of liquid electrolyte. Nevertheless, the efficiency of quasi-solid state DSSC still cannot reach the efficiencies of the conventional liquid electrolyte cells due to the poor contact of the solid-state charge transport material with the dye-coated TiO_2 surface (Günes, 2006). The I^- ion is more difficult to penetrate through the TiO_2 in the gel state. Kang et al. (2006) suggests to left the completed cells were at room temperature for 1 day in order for the electrolyte to penetrate in TiO_2 pores prior to photocurrent-voltage (IV) measurement.

Table 4.2: Comparison of gel and liquid MPN

	V_{oc} (V)	J_{sc} (mA/cm^2)	*FF*	η (%)
Gel	0.74	15.07	59.51	6.59
Liquid	0.73	14.15	68.21	7.01

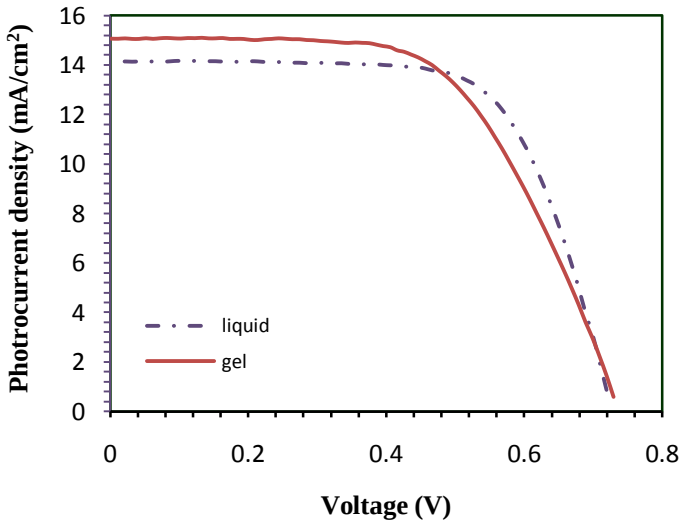

Figure 4.7: Photocurrent-voltage curve of gel and liquid MPN

4.3 Effect of Addictives on DSSC Performance

Researcher found that the precise composition of the triiodide/iodide electrolyte strongly affected the performance of the DSSC. Differences in composition would cause the charge recombination at TiO_2/electrolyte interface and the band edge movement of TiO_2 by the nature of the cation of iodide salt used. Therefore, additives were added into electrolyte to block the recombination centre (Lu et al., n.d.). Rijnberg et al. (n.d.) proposed that, additives help to prevent leakage of injected electron to the electrolyte, prevent I_3^- from approaching the surface of TiO_2 and suppress the loss of thiocyanto from the dye. The effect of GuSCN was shown clearly in the Figure 4.8.

Table 4.3: Comparison of the performance of ACN-based DSSC with and without additives and with GuSCN

	V_{oc} (V)	J_{sc} (mA/cm^2)	*FF*	η (%)
No additives	0.79	10.06	74.37	5.95
GuSCN	0.84	9.66	71.72	5.84

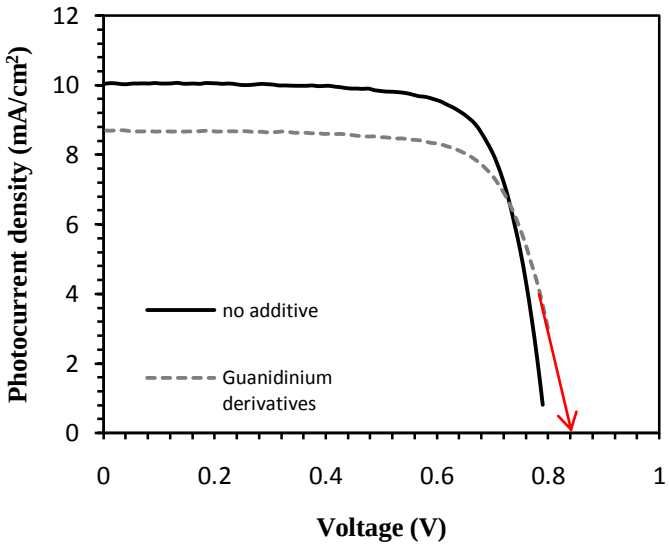

Figure 4.8: Photocurrent-voltage curve of ACN-based DSSC with and without GuSCN

Refer to Table 4.3, V_{oc} for DSSC with GuSCN is higher than that of without additive by 0.05V or 6.4%. This is because GuSCN suppresses the recombination rate of DSSC. Increase in V_{oc} will normally lead to increase in efficiency. (Dye Sensitized Solar Cells, n.d.) However, in this study, the result shows the other way. This might due to the lower *FF* of DSSC with GuSCN owing to the leakage of electrolyte and hence, results in lower efficiency.

Table 4.4: Comparison of the performance of ACN-based DSSC with and without pyridine derivative (TBP)

	V_{oc} (V)	J_{sc} (mA/cm^2)	FF	η (%)
No additives	0.7949	10.0572	74.3690	5.9453
TBP	0.8396	9.9501	73.9544	6.1780

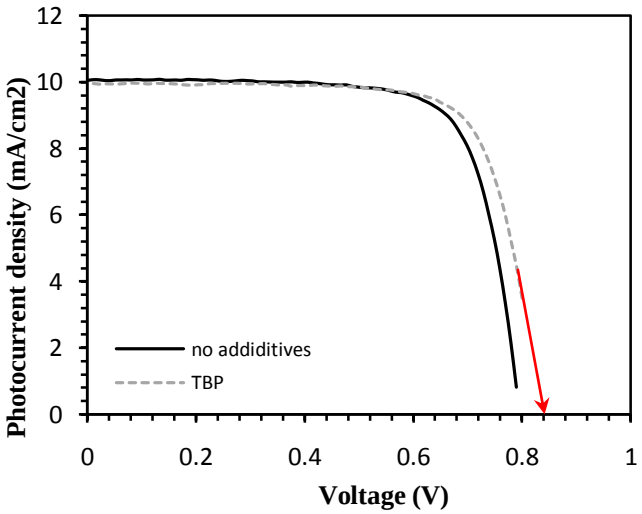

Figure 4.9: Photocurrent-voltage curve of ACN-based DSSC with and without TBP

TBP about 0.5M was added for most of the electrolyte and this is the concentration used in this study. Result in Table 4.4 shows that TBP able to increase the V_{oc} by 0.0447V or 5.6%. Based on Equation 4.1, the increases in V_{oc} will further lead to the increase of efficiency. Therefore, compare to the untreated cell, the DSSC with TBP has higher efficiency.

According to Lu et al. (n.d.), the increase of V_{oc} was contributed from the negative shift of Fermi level. This correlation can be explained by Figure 4.10. As shown in the figure, the voltage was generated due to the energy gap between the Fermi level of TiO_2 and the redox potential of the electrolyte mediator. When the Fermi level was shifted negatively, the maximum voltage increased, hence V_{oc} increased.

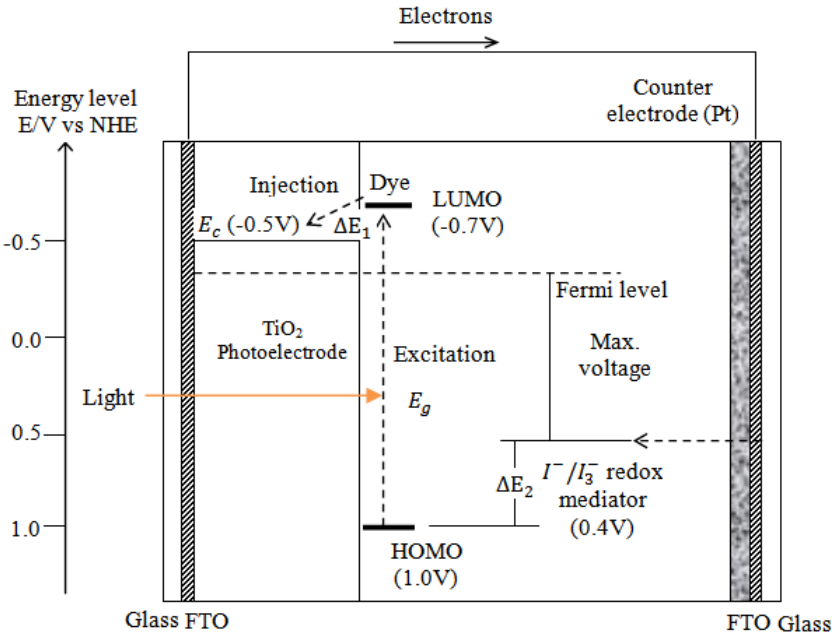

Figure 4.10: schematic energy diagram for DSSC

The energy gap between the LUMO and conduction band level of TiO_2, ΔE_1, is an important factor to determine the J_{sc} of DSSC. The energy level of LUMO must be sufficiently negative with respect to the conduction band of TiO_2. However, when TBP is added, conduction band (E_c) shifts negatively, reduces the ΔE_1. This cause the driving force of the electron injection from N719 LUMO to the conduction band of TiO_2 reduces, hence, J_{sc} decreases. Therefore, the energy gap ΔE_1 must be larger than approximately 0.2V as driving force for electron-transfer reaction to occur with optimal efficiency (Hara & Arawaka, 2003).

Based on Equation 4.1, when J_{sc} reduced, efficiency will be reduced. However, the reduction of J_{sc} was compensated by increase in V_{oc}. In this study, addition of TBP improves the V_{oc} and FF of DSSC and thus improves the efficiency of the cell as shown in Table 4.4.

M. Y. Li et al. (2007) found that the positive effect of pyridine derivatives on the V_{oc} and FF was due to the adsorption of pyridine groups on TiO_2 surface which induces electron density into the TiO_2 and creating a surface dipole. This results in suppression of the recombination of photogenerated electron from TiO_2 to triiodine in the electrolyte. Besides, addition of TBP protects the device from the usual

destructive effect due to the presence of water and probably results in a smaller reduction of J_{sc} (Rijnberg et al, n.d.).

4.4 Comparison of the performance for 4 DSSCs

Table 4.5 shows that V_{oc}, J_{sc}, FF and η are different for 4 similar DSSCs with TiO_2 metal oxide, N719 dye and MPN based electrolyte.

Table 4.5: I-V characteristic for sample A, B, C and D

	V_{oc} (V)	J_{sc} (mA/cm^2)	FF	η (%)
A	0.7321	10.1066	68.8034	5.0906
B	0.7568	11.7600	67.6369	6.0200
C	0.7260	14.1476	68.2089	7.0054
D	0.7581	15.9308	73.3363	8.8570

Sample D provided by Liu (2011)

The differences in DSSCs performance might be due to the crack formation in the TiO_2 paste of the cells as shown in the SEM micrograph (Figure 4.14). The formation of crack is due to the film shrinkage resulting from the evaporation and decomposition of organic substances and the considerable stress in the film induced by the volume change due to the crystallisation of TiO_2 (Ngamsinlapasathian et al., 2004). At the boundary of the crack, TiO_2 particle are not interconnected. This hinders the percolation of injected electrons thus reduces the efficiencies of certain cells.

Interconnection between first and second layer of the TiO_2 may affect the efficiency of the DSSC. When the connection between the TiO_2 is stronger, the efficiency of the DSSC will be higher. Poor contact between those layers hinders the electron transfer. SEM micrographs in Figure 4.14 show the poor connection between 2 layers of 20nm TiO_2 while Figure 4.15 shows a good connection of those

layers. Thus, sample D has the highest efficiency among the 4 samples. Furthermore, it is observed that the thickness of the TiO_2 layer is less than the optimum thickness (15 to 18 µm). Below optimum thickness, photocurrent generation is increase with increase in thickness. Therefore, J_{sc} is lower and η are negatively affected (Z. S. Wang et al., 2004).

4.5 XRD Analysis

To determine the phase identity and purity of TiO_2 used in this project, XRD is perform on the 20nm TiO_2 paste. Figure 4.11, shows the XRD patterns of single and double layers of the TiO_2. Both patterns display sharp peaks suggesting that they are crystalline in nature. Cell refinement was performed using "CHEKCELL" and all the peaks could be fully indexed as tetragonal with anatase structure confirming the formation of phase pure compound .Anatase phase is the preferred crystal polymorph as it results in larger maximum photovoltage. Therefore, the DSSCs can achieve better performance than that of DSSC with rutile TiO_2 (G. H. Li et al., 2009).

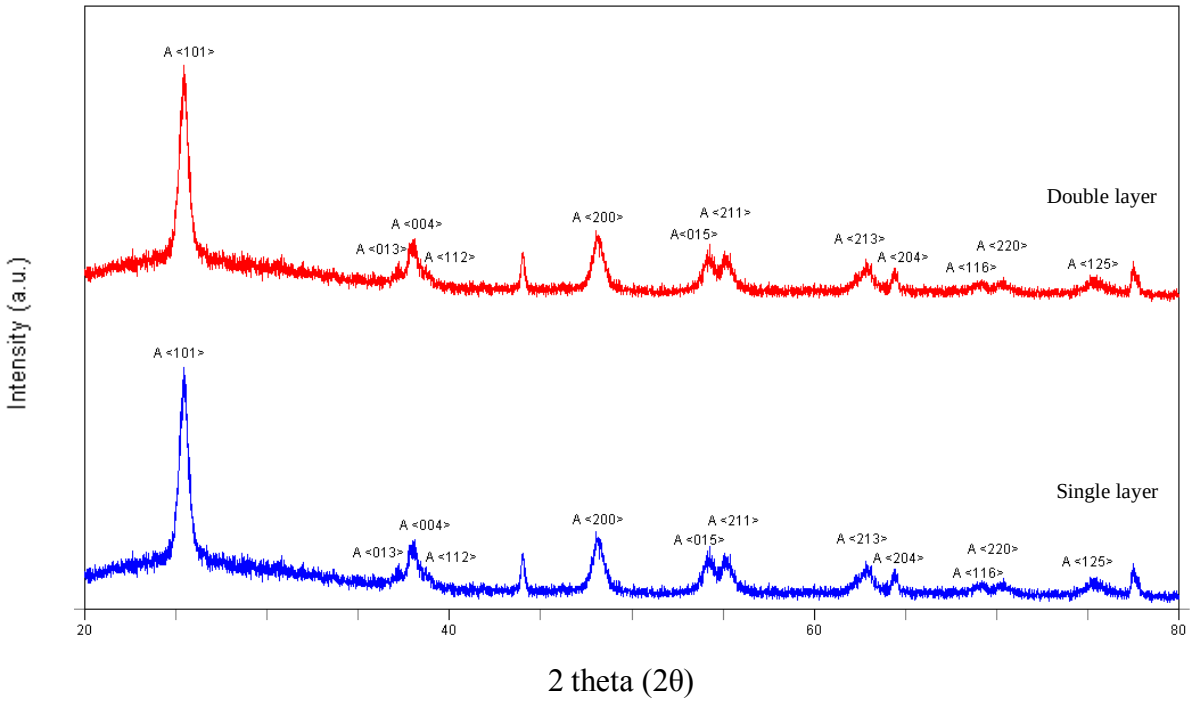

Figure 4.11: XRD pattern of single and double layers of 20 nm TiO_2

4.6 EDX

When other element is present in the paste, the conduction band of TiO_2 might be affected and it is not favourable for percolation of injected electrons. Consequently, it acts as the obstacle for electron transfer and performance of the DSSC will be affected.

Figure 4.12 shows the EDX result of a TiO_2 paste. From the result, it is proven that no other unwanted element is present in the TiO_2 paste used in this study. Small percentage of Carbon (C) might be coming from the carbon tape used for attachment of sample to the sample holder, finger print and contaminants in the air.

Table 4.6: Elements presented in TiO_2 paste

Element	Wt%	At%
C	01.23	02.84
O	34.60	59.99
Ti	64.17	37.16

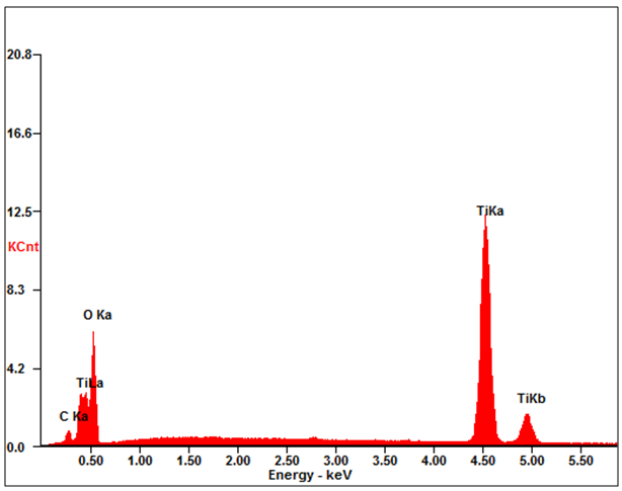

Figure 4.12: EDX result of TiO_2 paste

4.7 SEM

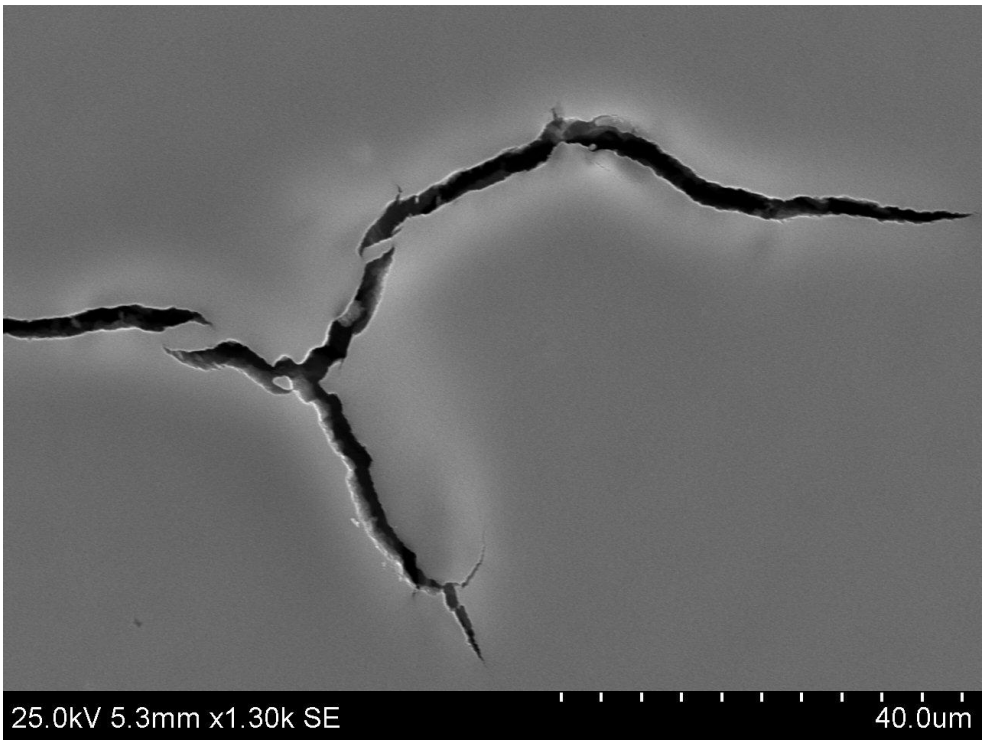

Figure 4.13: SEM micrograph of crack at the TiO_2 paste (1300 x magnification).

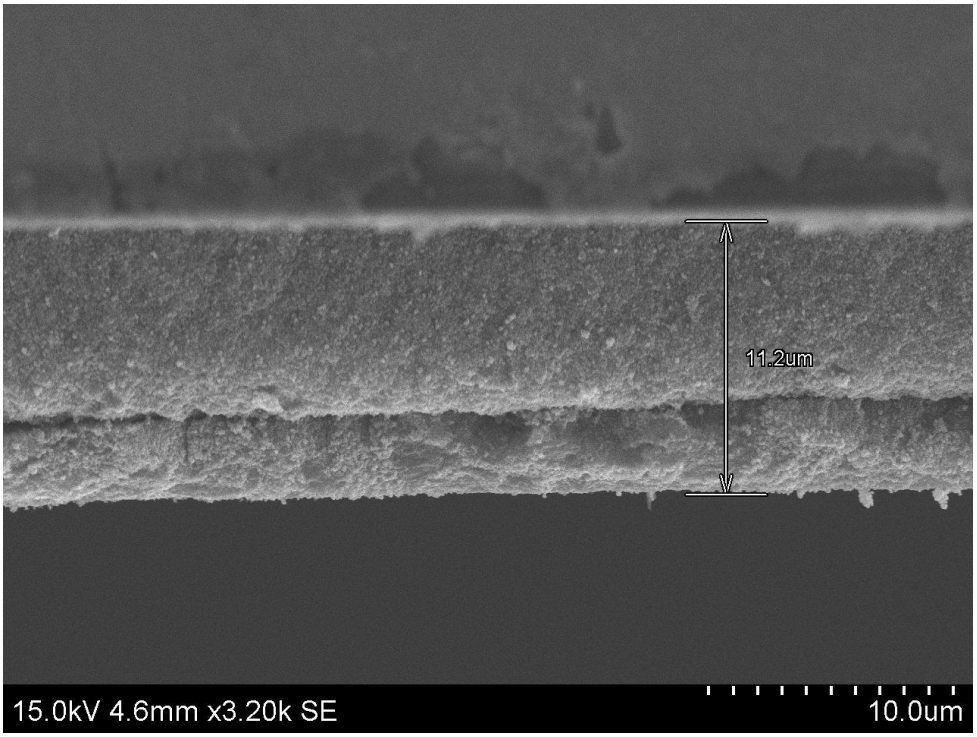

a

b

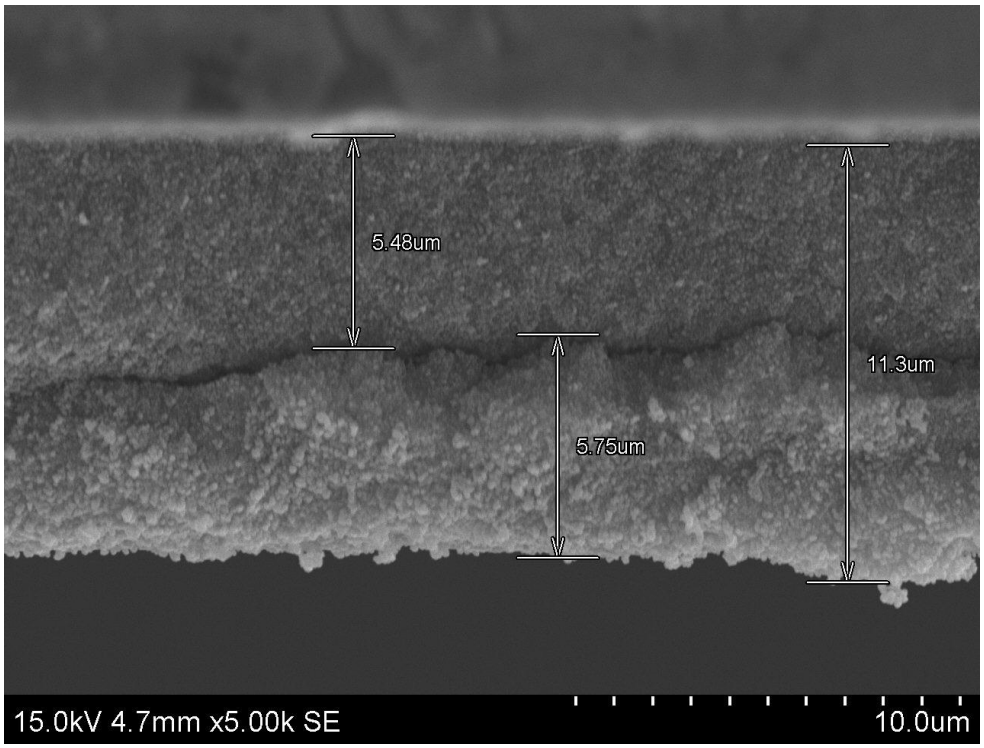

Figure 4.14: SEM micrograph of the sample A (a) 3200 x magnification (b) 5000 x magnification

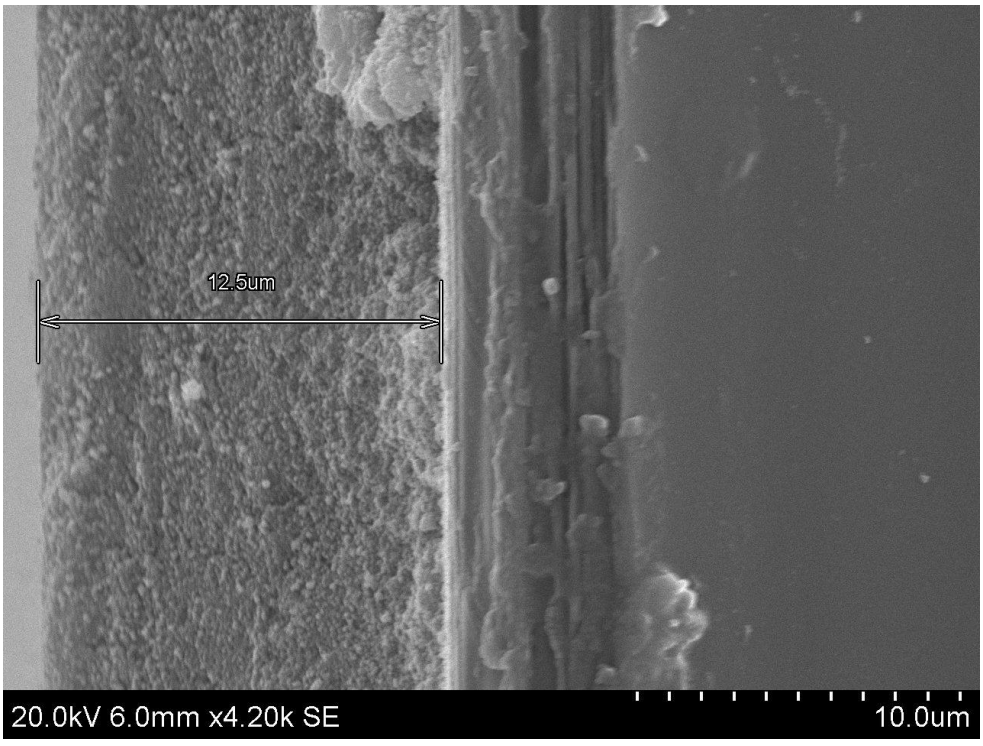

Figure 4.15: SEM micrograph of Sample D shows good bonding form between first and second layer of TiO_2 (4200 x magnification) (Liu, 2011)

CHAPTER 5

CONCLUSION AND RECOMMENDATIONS

5.1 Conclusion

The efficiency of the MPN-based electrolyte is higher than that of ACN-based electrolyte. However, according to the other researches, the ACN-based electrolyte should achieve a higher efficiency due to its formulations of relative low iodine concentration in the electrolyte. Therefore, it is suggested that the main cause for this difference is the fabrication process. On the other hand, higher iodine content in the MPN-based electrolyte improves its stability.

DSSC with the quasi-solid MPN-based electrolyte has lower efficiency than that of liquid MPN-based electrolyte due to poor contact of the quasi solid-state charge transport material with the dye-coated TiO_2 surface.

GuSCN is able to increase the V_{oc} of the solar cell by suppressing the recombination rate of DSSC. TBP yields the same result due to a negative conduction band movement; TBP adsorbed on the TiO_2 surface, its pyridine ring induces electron density into the TiO_2 and creating a surface dipole and suppresses the recombination of photogenerated electron from TiO_2 to triiodine in the electrolyte. However, J_{sc} of DSSC is lower than untreated cells. This is because the negative conduction band movement tends to reduce the driving force for electron injection to the TiO_2 conduction band.

A number of cells with the same combination (dye, metal oxide and electrolyte) are tested to check the consistency of their performance. Result that all the η obtained are different. The differences can be explained by the cracks at the surface of the TiO_2 and weak bonding between the layers of TiO_2 (gap). With cracks and gaps in the structure, percolation of injected electrons will be negatively affected and reduces the efficiency. Lastly, XRD for single and double layer TiO_2 shows that, TiO_2 used in the study consists of anatase phase.

5.2 Problem Encounter and Solution

5.2.1 Uneven Thickness

In this project, doctor blade technique is used to apply TiO_2 paste onto the glass substrate. Besides, the force that every different individual applied will be different as well. Therefore, the thickness for every sample will be different. This fact is show clearly by the colour of the paste during sintering.

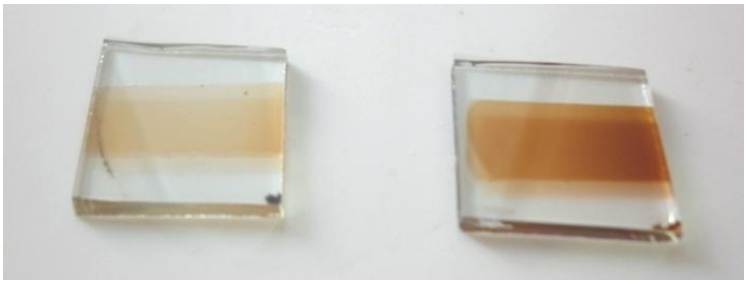

Figure 5.1: TiO_2-FTO glass which is heated at same temperature by using the same hot plate at the same time

Figure above show two samples which are made by the same paste with the same size which is TiO_2 paste with 20nm particle size. Both of the samples are sintered together by using the same hotplate at the same temperature in the same time. However, the colour of the paste is different. This is because the thicker layer tends to utilize more time to sinter the TiO_2 particle given the same temperature.

5.2.2 Glass Cutting Technique

In order to achieve best cutting (straight), there must be only one cutting line on the glass. Besides, the line must be depth enough. During cutting, the sound (zitz) must present. This sound represented that the glass have been cut.

If there are few lines on the glass and the cutting line is not deep enough, the glass will broke at where the force applied. In Figure 4.19, dash line represents the cutting line and red solid line is the path where glass broke. Therefore, poor cutting skill will result in irregular shape of FTO glass and wastage of FTO and Pt-coated glasses.

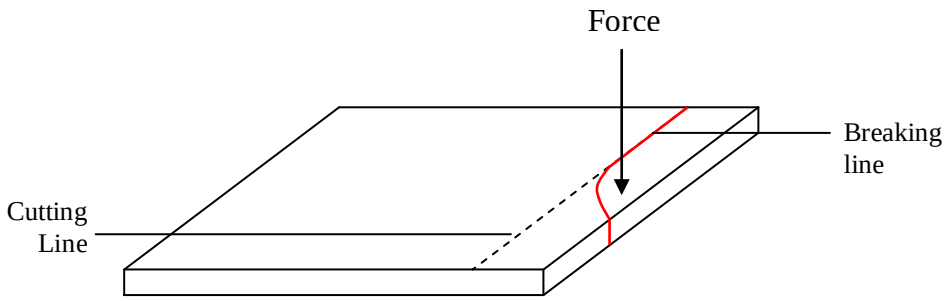

Figure 5.2: Path where glass broke due to poor cutting skill

5.2.3 Arc Lamp Power Supply Wire

The number of wire used in arc lamp power supply will affect the performance of DSSC. Figure below shows the I-V curve for the DSSC which used only 2 wires for arc lamp power supply. This DSSC uses TiO_2 as metal oxide, N719 as dye and ACN-based electrolyte. From voltage of 0V to 0.5V, the I-V curve is not smooth and it is fluctuated. Furthermore, at V_{oc} equal to 0.5, J_{sc} increase. This is not the normal trend. As show in other I-V curves in this chapter, the increase in voltage will cause decrease in photocurrent density. Therefore, 4 cables must be used in order to get the optimum result.

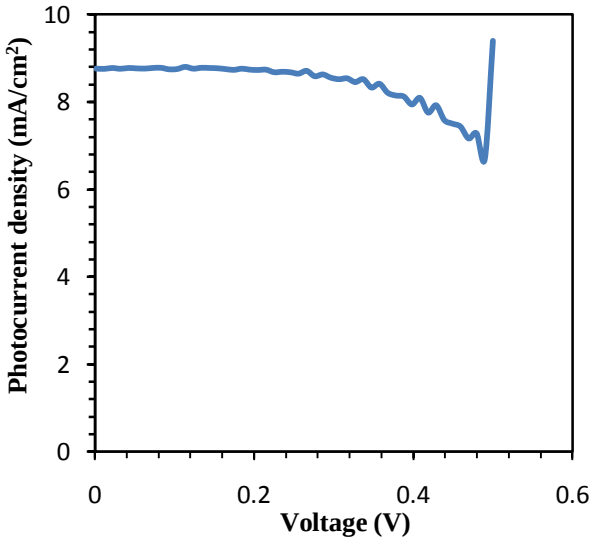

Figure 5.3: I-V curve for DSSC using 2 wires

5.3 Recommendation

In order to avoid the different thickness of the TiO_2 layer, spin coat method is recommended. This method is start by dripping the TiO2 paste onto the FTO surface by using pipette. After this, using spin coater, the substrate was spun at 3000 rpm for 30 s. The step is followed by soft-baked at 100ºC for 5 min and hard-baked at 300ºC for another 5 min. before carrying on with further coating The glass was allowed to cool down at room temperature to prevent to prevent cracks (Ong, 2009).

In this project, ACN based electrolyte is bought from Australia, while for MPN based electrolyte, it is fabricated in laboratory. This difference is the main factor that will affect the performance of the DSSC. Therefore, in order to obtain accurate result, both of the ACN and MPN based electrolyte should bought from Australia, or fabricated in laboratory.

For ACN based electrolyte, stability test is not able to carry due to quasi-solid ACN based electrolyte is not available. Therefore, for purpose of further research, quasi-solid ACN based electrolyte should be fabricated or bought from the Australia. Most importantly, if the electrolyte is bought from Australia, try to get all

electrolytes from the same company, if not, fabricate all in laboratory. This can reduce one parameter (fabrication process) which will affect the testing result and the performance of DSSC.

As discussed in section 2.2.3, sintering time and temperature is one of the parameter that will affect the efficiency of DSSC. The sintering time and temperature used in this project is not able to achieve the optimum performance of the DSSC. Therefore, the DSSC should sinter at 450˚C for 2 hour.

REFERENCES

An, H. L., Xue, B. F., Li, D. M., Li, H., Meng, Q. B., Guo, L., & Chen, L. Q. (2006). Environmentally friendly LiI/ethanol based gel electrolyte for dye-sensitized solar cells. *Electrochemistry Communications, 8*, 170-172.

Agilent Technologies. (2009). *PS-X10-100 solar cell I-V test system.* Retrieved August 11, 2010, from http://cp.literature.agilent.com/litweb/pdf/5990-4328ENA.pdf

Biancardo, M. (2006). *Incorporation of gel electrolyte in dye-sensitized solar cells could widen applications*. Retrieved November 23, 2010, from http://spie.org/documents/Newsroom/Imported/394/2006090394.PDF

Chen, Z. G., Yang, H., Li, X. H., Li, F. Y., Yi, T., & Huang, C. H. (2007). Thermostable succinonitrile-based gel electrolyte for efficient, long-life dye sensitized solar cells. *Journal of Materials Chemistry, 17*, 1602-1607.

Covalent Associates, Inc. (n.d.). *Introduction to ionic liquids*. Retrieved November 30, 2010, from http://www.covalentassociates.com/Introduction%20to%20Ionic%20Liquids.pdf

Dye sensitized solar cell. (n.d.). Retrieved July 3, 2010, from http://www.diss.fu-berlin.de/diss/servlets/MCRFileNodeServlet/FUDISS_derivate_000000002568/02_2.pdf?hosts=

Fernando, J. M. R. C., & Senadeera, G. K. R. (2008). Natural anthocyanins as photosensitizers for dye-sensitized solar devices. *Current Science, 95*(5), 663-666.

Grätzel, M. (2005). Mesocopic solar cells for electricity and hydrogen production from sunlight. *Chemistry Letters, 34*(1), 8.

Günes, D. I. S. (2006). Nanostructured electrodes from inorganic materials for hybrid solar cells. Unpublished PhD's thesis. Johannes Kepler Universität Linz, Austria.

Hara, K., & Arawaka, H. (2003). Dye-senitized solar cells. In *Handbook of Photovoltaic Science and Engineering* (p. 663). John Wiley &Sons Ltd.

Inakazu, F., Noma, Y., Ogomi, Y., & Hayasea, S. (2008). *Dye-sensitized solar cells consisting of dye-bilayer structure stained with two dyes for harvesting light of wide range of wavelength.* Retrieved June 13, 2010, from http://apl.aip.org/applab/v93/i9/p093304_s1?view=fulltext&display=print&bypassSSO=1

Kang, M. G., Kim, K. M., Ryu, K. S., Chang, S. H., Park, N. G., Hong, J. S., et al. (2004). Dye-sensitized TiO_2 solar cells using polymer gel electrolyte based on PVdF-HFP. *Journal of The Electrochemical Society*, *151*(2), E257-E260.

Koo, H. J., Park, J. H., Yoo, B. J., Yoo, K. C., Kim, K. K., & Park, N. G. (2008). Size-dependent scattering efficiency in dye-sensitized solar cell. *Inorganic Chimica Acta*, *361*, 677-683.

Krüger, J. (2003). Interface engineering in solid-state dye-sensitized solar cell. Unpublished PhD's thesis. Ecole Polytechnique Federale De Lausanne, Switzerland.

Lai, M. H., Tubtimtae, A., Lee, M. W., & Wang, G. J. (2010). ZnO-nanorod dye-sensitized solar cells: new structure without a transparent conducting oxide layer. *International Journal of Photoenergy*, *2010*.

Lai, W. H., Su, Y. H., Teoh, L. G., & Hon, M. H. (2008). Commercial and natural dyes as photosensitizers for a water-based dye-sensitized solar cell loaded with gold nanoparticles. *Journal of Photochemistry and Photobiology A: Chemistry*, *195*, 307–313.

Lenzmann, F. O., & Kroon, J. M. (2007). Review article: Recent advances in dye-sensitized solar cells. *Advances in OptoElectronics*, *2007*.

Leonardi, E. (2010). Sealing materials – encapsulation procedures and ageing tests for dye sensitized solar cell. Unpublished PhD's thesis. Università Degli Studi Di Roma "Tor Vergata", Italy.

Li, G. H., Richter, P. C., Milot, R. L., Cai, L., Schmuttebnaer, C. A., Crabtree, R. H. et al. (2009). Synergistic effect between anatase and rutile TiO_2 nanoparticles in dye-sensitized solar cells. *Dalton Transaction*, 10078–10085.

Li, M. Y., Feng, S. J., Fang, S. B., Xiao, X. R., Li, X. P., Zhou, X. W. et al. (2007). Quasi-solid state dye-sensitized solar cells based on pyridine or imidazole containing copolymer chemically crosslinked gel electrolytes. *Chinese Science Bulletin*, *52* (17), 2320-2325.

Lianos, P., Stathatos, E., Orel, B., Jese, R., Surca Vuk, A., & Jovanovski, V., (n.d.). *A quasi-solid state dye-sensitized solar cell based on a sol-gel nanocomposite electrolyte*. Retrieved December 18, 2010, from http://www.electrochem.org/dl/ma/203/pdfs/0147.pdf

Liu, C. C. (2011). Fabrication and characterisation of dye sensitized solar cell. Unpublished degree's thesis. Universiti Tunku Abdul Rahman, Malaysia.

Longo, C., & Paoli, M. A. (2003). Dye-sensitized solar cells: A successful combination of materials. *Journal of the Brazilizn Chemical Society*, *14*(6).

Lu, S. L., Koeppe, R., Günes, S., & Sariciftci, N. S. (2007). Quasi-solid state dye-sensitized solar cells with cyanoacrylate as electrolyte matrix. *Solar Energy Materials & Solar Cells, 91,* 1081–1086.

Lu, H. L., Li, Y. H., Huang, S. T., Su, C. C., & Thomas Yang, C. K. (n.d.). *Influences of water in bis-benzimidazole-derivative electrolyte additives to the degradation of the dye-sensitized solar cell*. Retrieved April 9, 2011, from http://www.cc.ntut.edu.tw/~wwwoaa/oaa-nwww/oaa-bt/bt-data/98_phd/paper/37.pdf

Ngamsinlapasathian, S., Sreethawong, T., Suzuki Y., & Yoshikawa, S. (2004). *Single- and double-layered mesoporous TiO_2/P25 TiO_2 electrode for dye-sensitized solar cell.* Retrieved June 25, 2010, from http://www.thaiscience.info/Article%20for%20ThaiScience/Article/3/Ts-3%20single-%20and%20double-layered%20mesoporous%20tio2p25%20tio2%20electrode%20for%20dye-sensitized%20solar%20cell.pdf

Ong, C. H. (2009). Conductive nanorod arrays for solar cells. Unpublished degree's thesis. Nanyang Technological University, Singapore.

Patch, K. (2004). *Solar cell doubles as battery*. Retrieved July 3, 2010, from http://www.trnmag.com/Stories/2004/120104/Solar_cell_doubles_as_battery_120104.html

PV Measurements, Inc. (2009). *I-V testing systems.* Retrieved August 11, 2010, from http://www.pvmeasurements.com/products/i-v-testing-system

Rijnberg, E., Kroon, J. M., Eienke, J., Hinsch, A., van Roosmalen, J. A. M., & Sinke, W. C. (n.d.). *Long-term stability of nanocrystalline dye sensitized solar cell.* Retrieved December 18, 2010, from http://www.ecn.nl/docs/library/report/1998/rx98033.pdf

Suryanarayanan, V., Lee, K. M., Ho, W. H., Chen, H. C., & Ho, K. C. (2007). A comparative study of gel polymer electrolytes based on PVdF-HFP and liquid electrolytes, containing imidazolinium ionic liquids of different carbon chain lengths in DSSCs. *Solar Energy Materials & Solar Cells, 91,* 1467-1471.

ScienceDaily. (2008). *New efficiency benchmark for dye-sensitized solar cell*. Retrieved August 11, 2010, from http://www.sciencedaily.com/releases/2008/06/080629130741.htm

Tan, B., & Wu, Y. Y., (2006). Dye-sensitized solar cells based on anatase TiO_2 nanoparticle/nanowire composites. *Journal of Physics and Chemistry, 110,* 15932-15938.

U.S. Department of Energy Office of Basic Energy Science. (2005). *Basic research needs for solar energy utilization*. Retrieved July 2, 2010, from http://www.science.deo.gov/bes/reports/files/SEU_rpt.pdf

Wang, P., Zakeeruddin, S. M., Moser, J. E., Nazeeruddin, M. K., Sekiguchi, T., & Grätzel, M. (2003). A stable quasi-solid-state dye-sensitized solar cell with an

amphiphilic ruthenium sensitizer and polymer gel electrolyte. *Nature Materials*, *2*, 402-406.

Wang, Z. S., Kawauchi, H., Kashima, T., & Arakawa, H. (2004). Significant influence of TiO_2 photoelectrode morphology on the energy conversion efficiency of N719 dye-senitized solar cell. *Cordination Chemistry Reviews*, *248*, 1381-1390.

Wongchareea, K., Meeyooa, V., & Sumaeth, C. (2007). *Dye-sensitized solar cell using natural dyes extracted from rosella and blue pea flowers.* Retrieved June 18, 2010, from http://www.energy-based.nrct.go.th/Article/Ts-3%20dye%20sensitized%20solar%20cell%20using%20natural%20dyes%20extracted%20from%20rosella%20and%20blue%20pea%20flowers.pdf

Wu, J. H., Lan, Z., Hao, S. C., Li, P. J., Lin, J. M., & Huang, M. L. (n.d.). *Progress on the polymer electrolytes for dye-sensitized solar cells.* Retrieved December 2, 2010, fom http://event09.ise-online.org/cdrom/files/ise082635.pdf

Xue, B. F., Wang, H. X., Hu, Y. S., Li, H., Wang, Z. X., Meng, Q. B., et al. (2004). An alternative ionic liquid based electrolyte for dye-sensitizedsolar cells. *Photochem. Photobiol. Sci.*, *3*, 918–919.

Yang, C. H., & Liao, S. H. (2009). Hydrothermal processed TiO_2 nanoparticles for optimization in dye-sensitized solar cells using statistical experimental strategies. *Physical and Analytical Electrochemistry (General)*, *19*(32), 3–20.

Yang, H. X., Huang, M. L., Wu, J. H., Lan, Z., Hao, S. C., & Lin, J. M. (2008). The polymer gel electrolyte based on poly(methyl methacrylate) and its application in quasi-solid-state dye sensitized solar cell. *Materials Chemistry and Physics*, *110*, 38-42.

Zhu, K., Neale, N. R., Miedaner, A., & Frank, A. J. (n.d.). *Oriented TiO_2 nanotube arrays for dye-sensitized solar cells:Effect of nanostructure order on transport, recombination, and light harvesting.* Retrieved June 18, 2010, from http://www1.eere.energy.gov/solar/review_meeting/pdfs/p_56_zhu_nrel.pdf

APPENDICES

APPENDIX A: Tables

In order to test the stability of ACN and MPN, 2 DSSCs have been fabricated which one of it using ACN-based electrolyte while the other used MPN-based electrolyte. Other parameter such as type of conductive glass, metal oxide and dye were remained constant. The conductive glass used was FTO glass and Pt-coated glass. The 20nm TiO_2 was chosen as the metal oxide. Lastly, the dye that used is N719. Table A shows the I-V characteristic for MPN over 32 days. I-V characteristic for ACN over 32 days are listed in Table B.

Table A: I-V characteristic for MPN- based electrolyte over a period of time

Day	V_{oc} (V)	J_{sc} (mA/cm^2)	*FF*	η (%)
1	0.6585	14.1995	69.7748	6.5243
2				
3				
4	0.7278	13.8036	71.1889	7.1519
5	0.7280	13.8056	71.2275	7.1588
6	0.7302	13.9371	70.7447	7.1995
7	0.7525	12.9789	71.1648	6.9508
8	0.7521	12.8009	71.5886	6.8926
9				
10				
11	0.7486	12.4093	71.7156	6.6622
12	0.7631	11.6254	72.0227	6.3897
13	0.7630	11.6215	72.6423	6.4416
14	0.7557	10.5202	73.1893	5.8187
15	0.7647	10.8278	73.2154	6.0620
16				
17				
18	0.7695	9.3577	73.3090	5.2786
19	0.7669	9.0729	72.6374	5.0540
20	0.7671	8.4558	72.5997	4.7091
21	0.7661	8.2654	72.9063	4.6164
22	0.7614	8.2566	72.3330	4.5474
23				
24				
25	0.7649	7.6374	73.4619	4.2913
26	0.7610	7.2245	73.0899	4.0184
27	0.7630	7.0425	73.0531	3.9254
28	0.7580	6.9105	73.2579	3.8374
29	0.7460	7.1864	73.5932	3.9456
30				
31				
32	0.7534	6.8346	74.1745	3.8196

Table B**: I-V characteristic for ACN- based electrolyte over a period of time**

Day	V_{oc} (V)	J_{sc} (mA/cm^2)	*FF*	η (%)
1	0.6905	9.8677	66.3498	4.5206
2				
3				
4	0.7538	9.6641	71.9187	5.2393
5	0.7857	8.9514	72.9871	5.1330
6	0.8148	5.4886	73.3892	3.2821
7	0.8606	6.0513	72.9730	3.8003
8	0.8072	5.9096	71.5540	3.6796
9				
10				
11	0.8594	7.0858	71.9025	4.3083
12	0.8925	6.5737	69.7732	4.0935
13	0.8844	5.7349	68.8946	3.4943
14	0.8743	4.5857	69.0138	2.7670
15	0.8910	4.4453	66.3842	2.6290
16				
17				
18	0.8453	2.9091	67.0798	1.6495
19	0.8668	3.0922	59.8912	1.6053
20	0.8777	2.7960	59.2097	1.4531
21	0.8506	2.3424	58.2970	1.1615
22	0.8380	1.7766	56.9945	0.8485
23				
24				
25	0.8505	1.9178	54.0063	0.8809
26	0.8362	1.4095	51.2138	0.6036
27	0.8277	1.2060	50.7174	0.5062
28	0.8243	1.0885	48.5100	0.4353
29	0.7503	0.4395	49.8008	0.1642
30				
31				
32	0.8337	0.2918	52.0698	0.1267